PERGAMON

Chaos, Solitons and Fractals 11 (2000) 2531–2560

CHAOS
SOLITONS & FRACTALS

www.elsevier.nl/locate/chaos

The dynamics of a triopoly Cournot game

Anna Agliari [a,b], Laura Gardini [b,c,*], Tönu Puu [d]

[a] *Catholic University in Milan, Italy*
[b] *University of Parma, Parma, Italy*
[c] *Istituto di Scienze Economiche, University of Urbino, 61029 Urbino, Italy*
[d] *Department of Economics, Umea University, S-901 87 Umea, Sweden*

Accepted 13 August 1999

Abstract

This paper reconsiders the Cournot oligopoly (noncooperative) game with iso-elastic demand and constant marginal costs, one of the rare cases where the reaction functions can be derived in closed form. It focuses the case of three competitors, and so also extends the critical line method for non-invertible maps to the study of critical surfaces in 3D. By this method the various bifurcations of the attractors and their basins are studied. As a special case the restriction of the map to an invariant plane when two of the three firms are identical is focused.

1. Introduction

Oligopoly, though contextually an intermediate situation between monopoly and perfect competition, is analytically a more complex case. The reason for this is that the oligopolist must consider not only the behaviors of the consumers, but also those of the competitors and their reactions. It is well known that the first formal theory of oligopoly goes back to A. Cournot, in 1838 [6], who treated the case with no retaliation at all, so that in every step each oligopolist assumes the last values taken by the competitors without any estimation of their future reactions. The adjustment process was assumed to lead to a fixed point, called Cournot equilibrium, independently of its stability character. More recent works have shown that the Cournot model may lead to cyclic behavior, and Rand proved in [28] that under suitable conditions the outcome may be chaotic. However his work does not include any economic assumption leading to this behavior. This was first done in [24,26], where such substantial assumptions were supplied in terms of an 'iso-elastic' demand function (i.e. reflecting a situation where the consumers always spend a constant sum on the commodity, regardless of price) and constant marginal costs. In the papers cited above only the duopoly case is considered, while in [25] a third producer is introduced (see also [27]), starting the study of a more complex situation, but also more interesting: a market with three oligopolists.

The recent interests among researches for the dynamics associated with repeated games is documented by the wide production on this subject (see, among others, [2–4,12,19]). In particular, in [10,11] it is shown how the analysis of the only attractors of a Cournot game may not be enough in order to understand the dynamical behaviors, and the role played by the global basins of attraction (which may have complex structure) is evidenced. We shall follow the same local–global approach.

The aim of our work is to study carefully the situation of a market with three oligopolists by an analysis of the local and global properties of the map describing the adjustment process, assuming the oligopolists

* Corresponding author. Fax: +39-722-327-655.
E-mail addresses: agliari@unipr.it (A. Agliari), gardini@econ.uniurb.it (L. Gardini), tonu.puu@econ.umu.se (T. Puu).

0960-0779/00/$ - see front matter
PII: S0960-0779(99)00160-5

adjusting their strategy simultaneously. Besides the local bifurcations, we investigate the basins of attraction of coexisting attracting sets, in some particular situations, making use of 'guided' numerical simulations, not only suitable but necessary due to the complexity of the model.

The paper is organized as follows. In Section 2 we introduce the three-dimensional model, defining the region of interest both for the mathematical system (admissible trajectories and region) and for the economic application (feasible trajectories and region). The local stability analysis on the unique Cournot equilibrium point is then recalled. In Section 3 we show some of the dynamics of interest, that is, how wide the basin of attraction may be, for the equilibrium point, when it is the only attractor, showing that the basin may become not simply connected, causing the appearance of non-admissible trajectories near the Cournot point. Also the coexistence of the stable Cournot point with a wide 'cycle' (really a closed invariant curve of the space), which attracts most of the feasible trajectories, is evidenced, announcing a Neimark–Hopf bifurcation of subcritical type. To understand the qualitative changes in the shape of the basin of attraction the critical surfaces of the map are used. These are introduced in Section 4. In Section 5 we prove some symmetry properties of the map, so that the three parameters of the model can actually be reduced to two, giving the topological conjugacy for the generic case. In Section 6 we study the dynamics of the model in the particular case in which two of the three marginal costs of the oligopolists are equal. In this case the asymptotic states belong to an invariant plane, on which the restriction of the map is simpler to analyze. It is shown that the three-dimensional basin undergoes a global bifurcation due to a contact between the critical plane and the boundary of the admissible region, and that the first contact is followed by other similar contacts causing the appearance of more 'holes' of non-admissible trajectories in the basin of attraction of the different kind of attraction set. Section 7 shows the topological conjugacies of the other possible cases with two equal marginal costs. The dynamic structure both of trajectories (enclosed inside an absorbing area completely determined) and of their basin of attraction, explained in the particular case, are then of help in understanding the generic cases with three different marginal costs considered in Section 8.

2. The model

We consider a Cournot oligopoly with three players. As in [24,25] we assume a demand function such that the price p is reciprocal to the total demand. Denoting by x, y and z the supplies of the competitors, the profits are, respectively, given by

$$U = \frac{x}{x+y+z} - ax, \quad V = \frac{y}{x+y+z} - by, \quad Z = \frac{z}{x+y+z} - cz, \tag{1}$$

where a, b and c represent the constant marginal costs of the oligopolists, and thus are positive parameters. In equilibrium, it is simple to obtain the reaction functions of the three oligopolists, given by

$$\begin{aligned} r_1(y,z) &= \sqrt{\frac{y+z}{a}} - y - z, \\ r_2(x,z) &= \sqrt{\frac{x+z}{b}} - x - z, \\ r_3(x,y) &= \sqrt{\frac{x+y}{c}} - x - y. \end{aligned} \tag{2}$$

Assuming, with Cournot, that the players move simultaneously at each stage of the game, by using their reaction function (2), we have the three-dimensional (3D henceforth) discrete model

$$T : \begin{cases} x' = \sqrt{\frac{y+z}{a}} - y - z, \\ y' = \sqrt{\frac{x+z}{b}} - x - z, \\ z' = \sqrt{\frac{x+y}{c}} - x - y, \end{cases} \tag{3}$$

where the symbol $'$ denotes the unit time advancement operator (i.e. if (x,y,z) represents the vector of choices at time t, then (x',y',z') gives the choices at time $(t+1)$). Our aim is to understand the dynamic behaviors of the map (3) as a function of the positive parameters (a,b,c) of the model. It is immediate to see that the map T is not defined in the whole three-dimensional space. The natural domain of definition of T is the region, say D, given by the set of points (x,y,z) which satisfy

$$D = \{(y+z) \geqslant 0,\ (x+z) \geqslant 0,\ (x+y) \geqslant 0\}. \tag{4}$$

But we have to consider a 'repeated' game, and thus we are interested in a subset of this set, which we call S, which consists in the points (x,y,z) for which we have $T^n(x,y,z) \in D$ for any $n \geqslant 0$. We shall call *admissible* such points and trajectories in S. However, not all the admissible trajectories are meaningful in our case. In fact, for the economic interpretation of the trajectories a negative value of a state variable is not acceptable, so that we have to restrict our interest to a lower set, which we shall call *feasible* points, denoted by F, of positive trajectories, that is, the locus of admissible points for which we have $T^n(x,y,z) \in S \cap \mathscr{R}^3_+$ for any $n \geqslant 0$ (and we shall can *infeasible* the other points and trajectories in S). Obviously $F \subseteq S \subseteq D$.

$$S = \{(x,y,z) \in D : T^n(x,y,z) \in D \text{ for any } n \geqslant 0\},$$
$$F = \{(x,y,z) \in S : T^n(x,y,z) \in S \cap \mathscr{R}^3_+ \text{ for any } n \geqslant 0\}.$$

The existence (and structure) of such a trapping region F of feasible trajectories is not easy to ascertain. We can be sure of its existence when the map T has an attracting (i.e. asymptotically stable) set belonging to $\mathscr{R}^3_+$ (fixed point or something else), and we shall see how it may be determined.

It is easy to verify that the *Cournot equilibrium* (Nash equilibrium of the game) is a fixed point of T, say E^*, given by

$$E^* = \left(\frac{2(-a+b+c)}{(a+b+c)^2}, \frac{2(a-b+c)}{(a+b+c)^2}, \frac{2(a+b-c)}{(a+b+c)^2} \right). \tag{5}$$

In order to analyze both when the fixed point is positive and its local stability character, it is suitable to consider the following ratios of the parameters:

$$h = \frac{b}{a}, \quad k = \frac{c}{a}. \tag{6}$$

Then, it follows immediately that $E^* \in \mathscr{R}^3_+$ (and being a fixed point we also have that $E^* \in S \cap \mathscr{R}^3_+$) iff

$$\begin{aligned} &h + k > 1, \\ &h - k < 1, \\ &h - k > -1 \end{aligned} \tag{7}$$

these relations detect a strip in the 'reduced' parameter plane (h,k) inside which h and k are let to vary in order to have admissible and feasible trajectories in our game (see Fig. 1).

The fixed points of T are the solutions of the algebraic system:

$$\begin{aligned} x &= \sqrt{\frac{y+z}{a}} - y - z, \\ y &= \sqrt{\frac{x+z}{b}} - x - z, \\ z &= \sqrt{\frac{x+y}{c}} - x - y, \end{aligned}$$

and besides the point E^* given above, also the origin satisfies these equations. However, the origin is not a feasible point, moreover, it is easy to see that the function T is not differentiable in such a point and a simple view of the Jacobian matrix of T, $J(x,y,z)$, given by

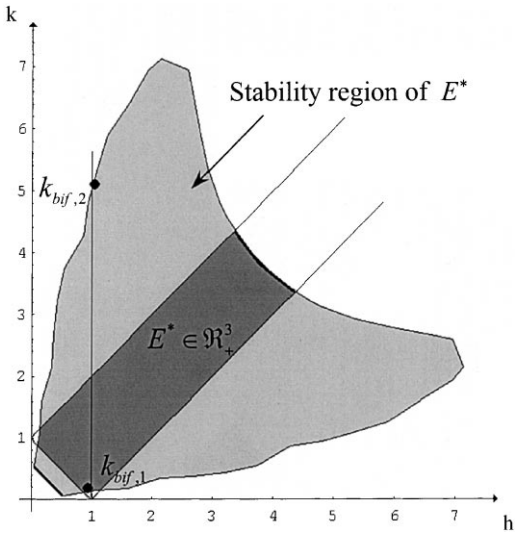

Fig. 1. Stability region of the Cournot point E^* in the 'reduced' parameter plane (h,k). In the dark gray strip, E^* is stable with positive coordinates. $k_{\text{bif},1}$ and $k_{\text{bif},2}$ are the bifurcation values for the 2D map obtained considering two producers with identical marginal costs (i.e. $h=1$).

$$J(x,y,z)=\begin{bmatrix} 0 & \dfrac{1}{2\sqrt{a(y+z)}}-1 & \dfrac{1}{2\sqrt{a(y+z)}}-1 \\ \dfrac{1}{2\sqrt{b(x+z)}}-1 & 0 & \dfrac{1}{2\sqrt{b(x+z)}}-1 \\ \dfrac{1}{2\sqrt{c(x+y)}}-1 & \dfrac{1}{2\sqrt{c(x+y)}}-1 & 0 \end{bmatrix} \tag{8}$$

shows that the eigenvalues of J tend to infinity as (x,y,z) tends to the origin. Thus we can consider the origin an unstable fixed point of the map. More difficult is to determine the stability conditions for the feasible fixed point E^*. The Jacobian matrix evaluated at E^* becomes

$$J^*=\begin{bmatrix} 0 & \dfrac{b+c-3a}{4a} & \dfrac{b+c-3a}{4a} \\ \dfrac{c+a-3b}{4b} & 0 & \dfrac{c+a-3b}{4b} \\ \dfrac{a+b-3c}{4c} & \dfrac{a+b-3c}{4c} & 0 \end{bmatrix}. \tag{9}$$

It turns out to be suitable to rewrite it as follows:

$$J^*=\begin{bmatrix} 0 & A & A \\ B & 0 & B \\ C & C & 0 \end{bmatrix}, \tag{10}$$

where

$$\begin{aligned} A&=\frac{h+k-3}{4}, \\ B&=\frac{k+1-3h}{4h}, \\ C&=\frac{1+h-3k}{4k}, \end{aligned} \tag{11}$$

while h and k are the reduced parameters defined in (6). Then, being $\mathrm{tr}(J^*) = 0$, and setting $D = \mathrm{Det}(J^*) = 2ABC, P = (AB + AC + CB)$, we get the characteristic polynomial

$$\mathrm{Det}(J^* - \lambda I) = p_3(\lambda) = -\lambda^3 + P\lambda + D. \tag{12}$$

By applying the Samuelson stability conditions (cf. [15]) to the polynomial (12), we get the following system of inequalities (which characterize the stability region of E^*):

$$\begin{aligned} &1 - P + D > 0, \\ &1 - P - D > 0, \\ &1 + P - D^2 > 0 \end{aligned} \tag{13}$$

a fourth condition being always satisfied. However, it is better to rewrite the conditions given in (13) substituting the expressions of P and D as a function of $A(h,k)$, $B(h,k)$ and $C(h,k)$ so that we can obtain a region in the reduced parameter plane (h,k). Avoiding such long explicit expressions, we give directly the outcome in the (h,k)-plane. It turns out that the second condition in (13) is always satisfied, while the last inequality implies the first one. Thus the stability region is obtained by use of the third condition only, and it is shown in Fig. 1, as obtained by use of a computer.

Its boundary is given by a curve crossing which we have a couple of complex eigenvalues whose modulus crosses the unitary value. This means that the loss of stability of E^* can only occur via a so-called Neimark–Hopf bifurcation, i.e. a couple of complex eigenvalues cross the unit circle in the complex plane, while the third real eigenvalue persists inside the unit circle. We shall investigate by the use of numerical simulations, by varying the marginal costs, the type of bifurcation that occurs, i.e. whether it is supercritical or subcritical. We recall that a Neimark–Hopf bifurcation is *supercritical* if crossing the bifurcation value the fixed point becomes unstable and a stable (i.e. attracting) closed invariant curve is created 'around' the unstable fixed point. It is *subcritical* if a repelling closed invariant curve exists around the stable fixed point, decreasing in size and merging with the fixed point at the bifurcation value 'transforming' it into an unstable one. The rigorous proof that the bifurcation is supercritical or subcritical requires a center manifold reduction (see e.g. [16]), which is not so simple in a 3D map, so that we shall detect the closed curves, either before or after the crossing of the stability region, by means of numerical evidence. We shall see that in the two arcs of interest for our applications, belonging to the strip of positivity of E^* (see the two arcs in Fig. 1, one on the lower left and one on the upper right of the strip), the bifurcation is always of subcritical type. Thus a repelling invariant closed curve appears around the stable fixed point, causing a sudden reduction of its basin of attraction. Crossing the bifurcation curve in other points it is possible to have a bifurcation of supercritical type, however we have never found it, that is, we have never seen the appearance of a stable curve around the unstable fixed point, also in the region of phase-space in which the trajectories, although admissible, are unfeasible.

3. Examples

Let us examine some of the dynamical phenomena of interest. Consider first the map T with parameters $(a,b,c) = (1, 3.8, 3)$ and increase c. For $c = 3$ we have the Cournot point E^* is the only attractor and its basin of attraction $\mathscr{B}(E^*)$ is a connected volume of $\mathscr{R}^3$ which also corresponds to the set of admissible trajectories S. We recall that the basin of an attractor is the set of points whose trajectories tend towards the attractor. A section of the basin on the plane through the fixed E^* and the z-axis, say Π^*:

$$\Pi^* : y = m^* x, \quad m^* = \frac{y^*}{x^*} = \frac{a - b + c}{-a + b + c} = \frac{1 - h + k}{-1 + h + k},$$

is shown in Fig. 2(a). The white points denote the set $S = \mathscr{B}(E^*)$, the gray points in D are the non-admissible points. A global bifurcation occurs as c increases, at which the basin from simply connected becomes connected with 'holes'. An example is shown in Fig. 2(b). The fixed point E^* is still the only attractor and a projection of its basin on the plane Π^* clearly shows a hole of non-admissible points, the

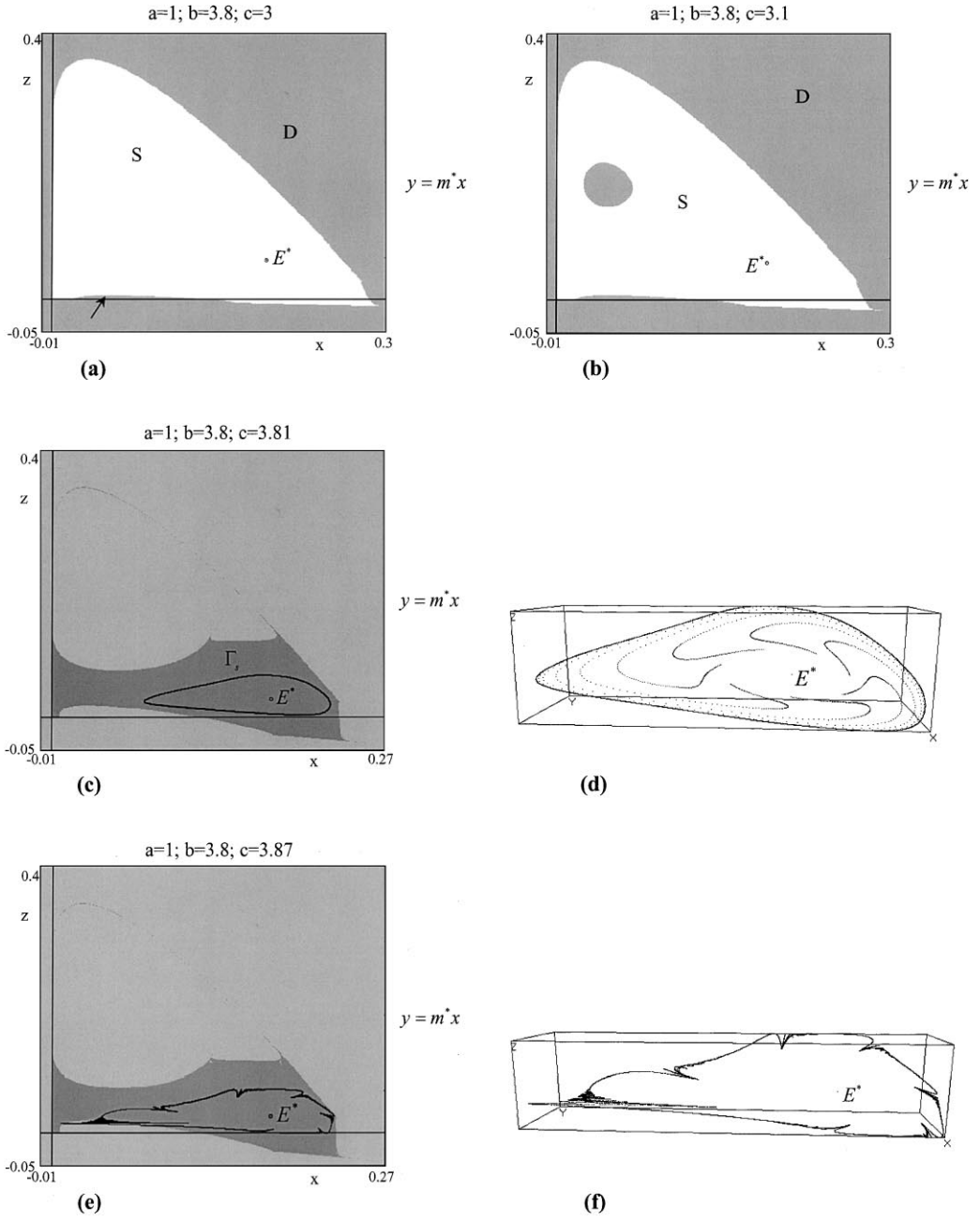

Fig. 2. (a) A section of the basin of the stable fixed point E^* on the plane through E^* and the z-axis ($y = m^*x$). The white points denote the set of admissible points, $S = \mathscr{B}(E^*)$, the gray points in D are the non-admissible points. (b) The section of the basin of E^* on the plane $y = m^*x$ shows a hole of non-admissible points, the gray points inside $\mathscr{B}(E^*)$. (c) The hole is bigger, and the attractor is now a closed invariant curve Γ_s whose basin is given by the dark gray region. (d) Three-dimensional representation of the closed invariant curve Γ_s. (e) A strange attractor obtained at a higher c value. On the plane $y = m^*x$, the section of its basin is given by the dark gray points. (f) Three-dimensional representation of the strange attractor.

gray points inside the basin $\mathscr{B}(E^*)$ which is still made up of the white points (and constitute the set of admissible trajectories S). In Fig. 2(c) the holes are bigger, and the attractor is a closed invariant curve Γ_s (see also Fig. 2(d)) whose origin, as we shall see, is not due to the crossing of the Neimark–Hopf bifurcation curve. A strange attractor is obtained at higher c values, an example is shown in Figs. 2(e) and 2(f). The projections are always of basins on the plane Π^*.

A similar sequence is observed decreasing c and crossing the bifurcation curve in the lower branch of Fig. 1. Consider the parameters $(a, b, c) = (1, 0.9, 0.35)$ and decrease c. For $c = 0.35$ we have a stable fixed point E^* and the set of admissible trajectories S is given by the white points in Fig. 3(a) (on the plane Π^*), which also gives the basin $\mathscr{B}(E^*)$, while the gray points in D represent non-admissible trajectories. In the phase-space $\mathscr{R}^3$ S is a simply connected volume, but as c decreases, again holes of non-admissible points appear inside S and increase in size (see Fig. 3(b) at $c = 0.25$). The set S coincides with the basin $\mathscr{B}(E^*)$ as long as the fixed point is the only attractor. In Fig. 3(c) we see that at $c = 0.24925$ two different attractors coexist, besides the stable focus E^*, also a closed invariant curve Γ_s is attracting, and it attracts most of the points in S (which is now the reunion of the two basins, $\mathscr{B}(E^*)$ and $\mathscr{B}(\Gamma_s)$). In the chosen plane Π^* the frontier of the basin $\mathscr{B}(E^*)$ is a closed curve, intersection of Π^* with a 3D closed surface, which seems homeomorphic to a sphere. In the 3D space this surface, or frontier, is the stable manifold of a repelling invariant closed curve. The presence of such a curve is due to a global bifurcation which gives simultaneous origin to two invariant closed curves, one attracting and the other repelling. Such a bifurcation (known as 'saddle-node for cycles') is quite common in flows, i.e. continuous time dynamical systems, but it does not happen so often in 3D discrete systems.

Comparing the basins of the fixed point E^* in Fig. 3(b) and (c) it is clear how such a global bifurcation corresponds also to a strong change in the basins of attraction of the fixed point, and from now, on decreasing the parameter c, we shall see a progressive reduction of the size of that basin. In fact, decreasing c the repelling closed curve reduces gradually in size, until it merges with the fixed point at the bifurcation value, turning it into repelling. It can be observed that setting the parameters near such a regime, the Cournot equilibrium is locally stable, but the feasible strategies converging to it are only those in a very small neighborhood of the equilibrium point, and the wider basin is that of the initial conditions leading to permanent cyclic strategies.

After the bifurcation value the attracting closed curve still exists, and turns into a chaotic attractor as c decreases. The study of these dynamics in the 3D space is not immediately intuitive, even if we know the critical surfaces (or manifolds) which bound a trapping region. In Fig. 3(d) the attractor is a chaotic set with a 3D structure, and we shall see that it can be enclosed inside an 'absorbing volume' in the phase-space, to which the chaotic set is tangent. Fig. 3(e) will be explained later, after the introduction of the critical surfaces and the inverses of the map.

In order to better understand the dynamics of the model, in Section 6 we shall consider the particular case obtained assuming that two producers have the same marginal costs ($a = b$). In such a situation, the plane $x = y$ is invariant under the map (3). For the points belonging to that plane the dynamics can be studied by use of the restriction of T to the plane, which is a two-dimensional (2D henceforth) map, easier to analyze. Regarding the dynamics in the 3D space it can be shown that the invariant plane attracts many feasible trajectories, being the transverse eigenvalues less than 1 in modulus. This example is noticeable because it permits to better understand the global bifurcations which change the structure both of the attractors and of the basins. Then it is easy to extend the results to the generic case.

Another important result, obtained by using the restriction of the map to the invariant plane, is related to the region of admissible trajectories. We study the global bifurcations of such a region by means of the critical curves and their contacts with the frontier of the region. Again these results may be extended to the general case, for example, the bifurcations in the basins seen in the examples of this section will be explained by using the critical surfaces of T.

4. The critical surfaces and the inverses of T

Some of the global bifurcations which cause changes in the basins of attraction can be explained making use of the critical planes and critical surfaces of the map. It is easy to see that our model is a noninvertible one, i.e. even if one point $(x, y, z) \in S$ is uniquely mapped into a point $(x', y', z') = T(x, y, z)$, the rank-1 preimage of a point (x', y', z') belonging to S may not exist or may be a set of finite number of distinct points. Following [17,21], we recall that the critical points of rank-0 are points in which the Jacobian matrix of T vanishes and the map is not locally invertible. The set of such points are called Critical Surfaces (CS), of rank-0, and denoted by CS_{-1} (or critical manifolds, our map being a 3D one, while they are called critical

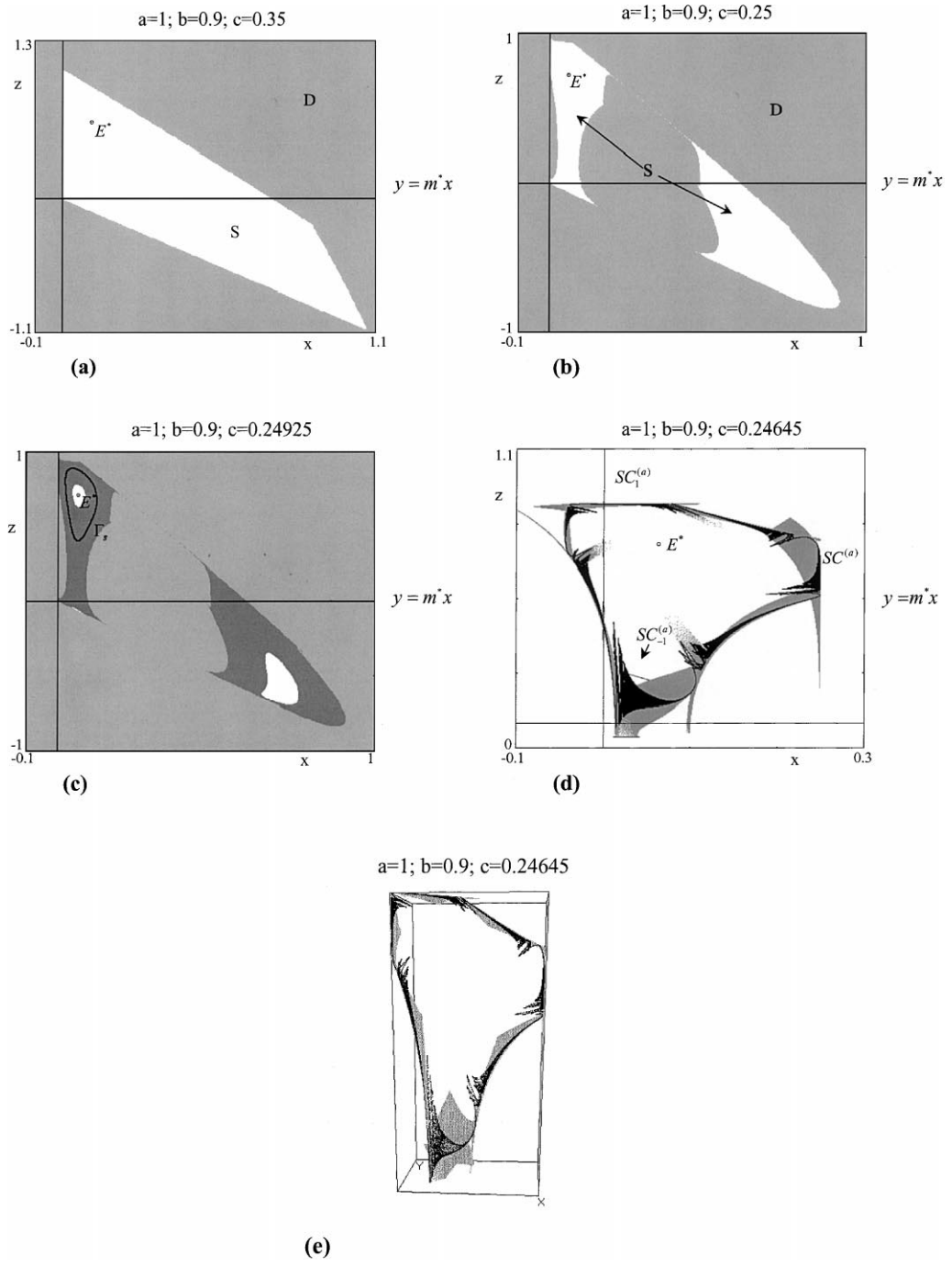

Fig. 3. (a) For a different choices of the parameters (given in figure) E^* is still a stable fixed point. The set of admissible trajectories S on the plane $y = m^*x$ is given by the white points, which also gives the basin $\mathscr{B}(E^*)$. The gray points D represent non-admissible trajectories. (b) On decreasing c, holes of non-admissible points appear inside S. (c) Two different attractors coexist: the stable focus E^* and an attractive closed invariant curve Γ_s born via a 'saddle-node for cycles' bifurcation. Now S, still projected on the plane $y = m^*x$, is the reunion of the two basins, $\mathscr{B}(E^*)$, white points, and $\mathscr{B}(\Gamma_s)$, dark gray points. The frontier of $\mathscr{B}(E^*)$ is a repelling closed curve. (d) For smaller values of c, E^* becomes unstable via a subcritical Neymark–Hopf bifurcation and Γ_s turns into a chaotic attractor. Here the gray points are the projection on the plane $y = m^*x$ of an absorbing volume, bounded by portions of critical surfaces. (e) The three-dimensional representation of the chaotic set with the absorbing volume.

curves and critical points in maps of dimension two and one, respectively). From the Jacobian matrix given above (8) we have

$$\mathrm{Det}(J(x,y,z)) = 2\left(\frac{1}{2\sqrt{a(y+z)}}-1\right)\left(\frac{1}{2\sqrt{b(x+z)}}-1\right)\left(\frac{1}{2\sqrt{c(x+y)}}-1\right)$$

so that the locus $\mathrm{Det}(J(x,y,z))=0$ is made up of three planes, portions of which constitute our critical set CS_{-1} of rank-0, which is made up of the intersections of the domain of T with the planes of equation: $y+z=1/4a,\ x+z=1/4b,\ x+y=1/4c$. In order to distinguish the different components of the critical sets we shall call $\mathrm{CS}_{-1}^{(a)}$ the portion of the domain of T on the plane of equation $y+z=1/4a$, $\mathrm{CS}_{-1}^{(b)}$ that on the plane $x+z=1/4b$ and $\mathrm{CS}_{-1}^{(c)}$ the one on $x+y=1/4c$, so that we have $\mathrm{CS}_{-1}=\mathrm{CS}_{-1}^{(a)}\cup\mathrm{CS}_{-1}^{(b)}\cup\mathrm{CS}_{-1}^{(c)}$,

$$\mathrm{CS}_{-1}^{(a)} = D\cap\left\{y+z=\frac{1}{4a}\right\},$$

$$\mathrm{CS}_{-1}^{(b)} = D\cap\left\{x+z=\frac{1}{4b}\right\},$$

$$\mathrm{CS}_{-1}^{(c)} = D\cap\left\{x+y=\frac{1}{4c}\right\}.$$

The images by T of such portions of planes are critical surfaces of rank-1, say $\mathrm{CS}=T(\mathrm{CS}_{-1})$ where we shall distinguish the three surfaces $\mathrm{CS}^{(l)}=T(\mathrm{CS}_{-1}^{(l)})$ for $l=a,b$ and c. It is easy to see that the three surfaces $\mathrm{CS}^{(l)}$ are portions of planes:

$$\mathrm{CS}^{(a)} \text{ belongs to the plane } x=\frac{1}{4a},$$
$$\mathrm{CS}^{(b)} \text{ belongs to the plane } y=\frac{1}{4b},$$
$$\mathrm{CS}^{(c)} \text{ belongs to the plane } z=\frac{1}{4c}.$$

We recall that the CS generally separate regions (or zones) of the phase-space, the points of which have a different number of distinct rank-1 preimages, and that crossing through a critical surface the number of rank-1 preimages changes by 2 or a multiple of 2. In order to understand which are the preimages, and how many, we have to solve the system in (3) assuming given an admissible point (x',y',z') and searching for the possible solution vectors (x,y,z). To do this let us define $\alpha=\sqrt{x+y},\ \beta=\sqrt{x+z},\ \gamma=\sqrt{y+z}$, then we have

$$\alpha_{\pm} = \frac{1\pm\sqrt{1-4cz'}}{2\sqrt{c}} \quad \text{if } 0\leqslant z'<\frac{1}{4c},$$
$$\alpha = \frac{1+\sqrt{1-4cz'}}{2\sqrt{c}} \quad \text{if } z'<0,$$

$$\beta_{\pm} = \frac{1\pm\sqrt{1-4by'}}{2\sqrt{b}} \quad \text{if } 0\leqslant y'<\frac{1}{4b},$$
$$\beta = \frac{1+\sqrt{1-4by'}}{2\sqrt{b}} \quad \text{if } y'<0,$$

$$\gamma_{\pm} = \frac{1\pm\sqrt{1-4ax'}}{2\sqrt{a}} \quad \text{if } 0\leqslant x'<\frac{1}{4a},$$
$$\gamma = \frac{1+\sqrt{1-4ax'}}{2\sqrt{a}} \quad \text{if } x'<0,$$

so that, given any tern (α,β,γ) from the relations above we have one of the inverses of T which reads as

$$T^{-1}(x',y',z')=\left(\frac{\alpha^2+\beta^2-\gamma^2}{2},\ \frac{\alpha^2-\beta^2+\gamma^2}{2},\ \frac{-\alpha^2+\beta^2+\gamma^2}{2}\right). \tag{14}$$

Noticing that an admissible point (x',y',z') can have at most one negative component (because from (4) it follows that the sum of any two components must be positive), we obtain several zones in the admissible region of the phase-space, as stated in the following proposition, where the notation Z_k is used to denote a region whose points have k distinct rank-1 preimages.

Proposition 1. *Let (x,y,z) be an admissible point, then*

(i) *Z_0 is the region of space for which $z>1/4c$ or $y>1/4b$* or *$x>1/4a$*;

(ii) *Z_8 is the region of space bounded by the critical planes of equation $z=1/4c,\ y=1/4b,\ x=1/4a$, and the coordinate planes*;

(iii) *Z_4 are the intersections of the admissible region with the three ortants of the space whose points have one and only one negative component*.

From the above proposition it follows that the planes of equation $z=1/4c,\ y=1/4b,\ x=1/4a$ or, more rigorously, their proposition not belonging to Z_0 constituting $\mathrm{CS}(\mathrm{CS}=\mathrm{CS}^{(a)}\cup\mathrm{CS}^{(b)}\cup\mathrm{CS}^{(c)})$ are critical surfaces of rank-1 in the usual sense. That is, any point (x',y',z') belonging to such a critical surface $\mathrm{CS}^{(l)}$ has at least two merging rank-1 preimages belonging to the critical surface $\mathrm{CS}^{(l)}_{-1}$ which, in its turn, is made up of points in which the Jacobian determinant of T vanishes. Such points of CS separate the region Z_0 with zero rank-1 preimages from a region having either 8 or 4 distinct rank-1 preimages, i.e. Z_0-Z_8 or Z_0-Z_4. For example, consider a point $p'=(x',y',1/4c)$ belonging to the critical surface $\mathrm{CS}^{(c)}(z=1/4c)$, then its rank-1 preimages $T^{-1}(x',y',1/4c)$ include (being $\alpha_-=\alpha_+$) couples of two merging preimages which are obtained by considered the tern of values $(\alpha_-,\beta_\pm,\gamma_\pm)=(\alpha_\pm,\beta_\pm,\gamma_\pm)$ giving either four or two points (depending on $p'\in\partial Z_8$ or $p'\in\partial Z_4$), and from (14), all the merging preimages belong to the critical plane $\mathrm{CS}^{(c)}_{-1}(x+y=1/4c)$.

The coordinate planes, although playing a role of 'separation' between zones with different preimages (the portions not in Z_0 separate Z_8-Z_4) are not critical surfaces. This is due to the fact that the domain of definition of our map T is not the whole space, because of the square roots in its definition which imply the constraints given in (4). In the same way, also the explicit formulation of the inverses (which can be obtained from the relations given above) all have a square root in their definitions, and it happens that eight inverses are defined in Z_8 while only four of them exist in Z_4. *The points belonging to a coordinate plane have not merging rank-1 preimages belonging to a critical surface*. Such points still belong to the region with eight distinct rank-1 preimages. An example for all: the origin $O=(0,0,0)$ belongs to Z_8 and its eight distinct (i.e. disjoint) rank-1 preimages are:

$$\begin{aligned}
O_{-1,1}&=(0,0,0)\\
O_{-1,2}&=\left(-\frac{1}{2a},\frac{1}{2a},\frac{1}{2a}\right)\\
O_{-1,3}&=\left(\frac{1}{2b},-\frac{1}{2b},\frac{1}{2b}\right)\\
O_{-1,4}&=\left(\frac{1}{2c},\frac{1}{2c},-\frac{1}{2c}\right)\\
O_{-1,5}&=\left(\frac{1}{2b}-\frac{1}{2a},-\frac{1}{2b}+\frac{1}{2a},\frac{1}{2b}+\frac{1}{2a}\right)\\
O_{-1,6}&=\left(\frac{1}{2c}-\frac{1}{2a},\frac{1}{2c}+\frac{1}{2a},-\frac{1}{2c}+\frac{1}{2a}\right)
\end{aligned}$$

$$O_{-1,7} = \left(\frac{1}{2c}+\frac{1}{2b},\frac{1}{2c}-\frac{1}{2b},-\frac{1}{2c}+\frac{1}{2b}\right)$$
$$O_{-1,8} = \left(\frac{1}{2c}+\frac{1}{2b}-\frac{1}{2a},\frac{1}{2c}-\frac{1}{2b}+\frac{1}{2a},-\frac{1}{2c}+\frac{1}{2b}+\frac{1}{2a}\right).$$

Note that such eight rank-1 preimages of the origin continue to be distinct even if some of the parameters have the same value, also when $a = b = c$.

Finally we remark that even if the points in the regions Z_4 may be admissible, they are certainly not feasible (such points having one negative component). It is suitable at first, to consider the whole dynamics of the map T, and then we will turn to consider the positivity condition on the state variables.

Besides the critical planes $\mathrm{CS} = T(\mathrm{CS}_{-1})$, also the images of higher rank of the critical set CS_{-1} are called critical. As usual, we shall call critical set of rank-$(k+1)$ for $k \geqslant 0$, the image of rank-$(k+1)$ of CS_{-1}, or, equivalently, the image of rank-k of CS, denoting it as CS_k, that is, $\mathrm{CS}_k = T^K(\mathrm{CS}) = T^{k+1}(\mathrm{CS}_{-1})$ (CS_0 being equal to CS). It is clear that in our example the critical set of given rank is always made up of three components, namely:

$$\mathrm{CS}_k^{(l)} = T^k(\mathrm{CS}^{(l)}) = T^{k+1}(\mathrm{CS}_{-1}^{(l)}) \quad \text{for } l = a, b, c.$$

The role played by the critical points in non-invertible maps is well documented for the 2D case (we refer to [21] and references therein for a survey of several results, many of which dates back to [17]) and also in one-dimensional maps, not only unimodal (see the kneading theory in [14,18]).

One of the more fascinating (as well as useful) applications of the critical curves in 2D maps is that by a finite number of segments of critical curves we can obtain exactly the boundary of absorbing areas. An absorbing area A is trapping (i.e. mapped into itself by application of the map), and absorbing (i.e. a basin $\mathscr{B}(A)$ exists, which includes a neighbourhood of A, made up of points whose trajectory tends to A). Generally (i.e. except for particular bifurcation cases in the set of parameters defining the map) all the trajectories enter A in a finite number of applications of the map (and then can never escape). Often the absorbing area is invariant, which means mapped exactly into itself by an application of the map ($T(A) = A$). An example of such a 2D absorbing area will be shown in Section 6.

It is obvious how such properties read in the case of a 3D non-invertible map, as it is our case. Fig. 3(d) and (e) represent an 'absorbing volume', bounded by a finite number of portions of 'critical surfaces' $\mathrm{CS}_i^{(l)}$ $i \geqslant 0$, and the chaotic attractor inside it, which has a 3D structure. Following (and extending) the procedure outlined in [21, ch. 4], we have selected a portion of critical surfaces $\mathrm{CS}_{-1}^{(l)}$ which is crossed by the attractor. Then by a finite number of images, we completely cover the external boundary of a closed trapping volume V (so that $T(V) \subseteq V$), which is absorbing, because all the initial conditions in a neighborhood of V have trajectories which enter V in a finite number of iterations. Moreover, in the example shown in that figure the absorbing volume is invariant, i.e. $T(V) = V$, and the external boundary is obtained by taking seven images of a portion of $\mathrm{CS}_{-1}^{(a)}$. Moreover, we could also construct a trapping 'annular volume' V_a (a geometric structure which reminds a torus, even if it may be, or not, homeomorphic to a torus). Such a volume has an empty space inside it, or 'spherical-hole', made up of points which, except for at most a set of zero measure, have the trajectories which enter the annular volume and never escape. Also the boundary of the annular volume is made up of a finite number of images of a portion of a critical surface. It is the 3D analog of a 2D annular absorbing area (as we shall see in Section 6).

It is worth noticing the advantage coming from the knowledge of such an absorbing volume in the applied context, specially when the attracting set is chaotic. In fact, in such cases it is not possible to predict (i.e. forecast) the value of the state variables (although the model is deterministic). But the knowledge of an absorbing volume gives an element of certainty: the width of the interval of variation is known, as well as, often, also the qualitative structure of the trajectories (for example, it is often possible to forecast if there will be an increase or decrease in the state variables).

Another useful application of the critical curves in 2D non-invertible maps is related to the bifurcations which cause qualitative changes in the structure of basins of attractions. As a germinal paper on this subject we refer to [22], and in extended form to [1,21], while several detailed examples have been recently published [5,7–9,13,20]. It is obvious that also in 3D non-invertible maps we can see this very important type of

applications. Indeed, these kinds of bifurcations are those which cause non-connected basins and complexity in the basin-structure (i.e. not only on the boundary). The basins shown in Figs. 2 and 3 of Section 3 are a clear demonstration of the occurrence of such bifurcations. Our aim is to explain such phenomena, showing the contact bifurcations which cause changes in the basins structure. In order to better explain these phenomena we shall consider some particular cases of our 3D map, which are obtained when two of the oligopolists are similar: they reason in the same way. This case occurs when two of the oligopolists are similar: they reason in the same way. This case occurs when two of the three parameters are equal. Let us first examine, in Section 5, some basic properties of T as a function of the parameters.

5. Topological conjugacy and symmetry properties

That the three parameters of the map are not all independent from a dynamical point of view comes from the following proposition:

Proposition 2. *The dynamics of the map T with terns of parameters (a, b, c) and $(\tau a, \tau b, \tau c)$ with $\tau > 0$ are topologically conjugate, via the homeomorphism $\phi(x, y, z) = (\tau x, \tau y, \tau z)$.*

In fact, it is easy to see that if we change the three parameters (a, b, c) into $(\tau a, \tau b, \tau c)$ with $\tau > 0$, then we obtain a 3D map, say $\tilde{T}$ which is topologically conjugate with the map T by use of the homeomorphism $\phi(x, y, z) = (\tau x, \tau y, \tau z)$, being $\tilde{T} = \phi^{-1} \circ T \circ \phi$ (or equivalently $T = \phi \circ \tilde{T} \circ \phi^{-1}$). This means that the trajectories of the map $\tilde{T}$ are obtained from those of the map T by applying the transformation $\phi^{-1}(x, y, z) = (x/\tau,\ y/\tau,\ z/\tau)$ to all the points of any trajectory, or equivalently, the trajectories of the map T are obtained from those of the map $\tilde{T}$ by applying the transformation $\phi(x, y, z) = (\tau x, \tau y, \tau z)$.

Note that the homeomorphism used in the above proposition transforms admissible trajectories (whose points are always in the domain of definition of the map) into admissible trajectories, and feasible trajectories (whose points are all in the positive orthant) into feasible trajectories. Clearly this is a simple consequence of the conjugacy, if S (resp. F) is the considered set of $\tilde{T}$ then $\phi(S)$ (resp. $\phi(F)$) is the corresponding set of T.

From this proposition it follows that the *reduced parameters* of the map, h and k defined in (6), are the two essential independent parameters which we vary in order to investigate the dynamic behaviors of the map, as the dynamics in the phase-space associated with the tern (a, b, c) are the same as (i.e. are topologically conjugate to) those of the map obtained with the parameters $(1, h, k)$.

Another symmetry is immediately evident also in the reduced parameter plane, that is, the bifurcation curves in the plane (h, k) must be symmetric with respect to the bisectrix $(h = k)$ (as it was evident also from Fig. 1). This comes from the following proposition:

Proposition 3. *The dynamics of the map T with terns of parameters $(1, h, k)$ and $(1, k, h)$ are topologically conjugate, via the homeomorphism $\psi_1(x, y, z) = (x, z, y)$.*

In fact, it is easy to see that if we change three parameters $(1, h, k)$ into $(1, k, h)$, then we obtain a 3D map, say $\overline{T}$ which is topologically conjugate to the map T by use of the homeomorphism $\psi_1(x, y, z)$, being $\overline{T} = \psi \circ T \circ \psi_1$ or equivalent $T = \psi_1 \circ \overline{T} \circ \psi_1$, as $\psi_1^{-1} = \psi_1$. This means that the trajectories of the map $\overline{T}$ and those of T are transformed one into the other by the transformation $\psi_1(x, y, z) = (x, z, y)$.

From the property given above we have another immediate consequence, a symmetry property which holds in the case of identical reduced parameters $h = k$. In this case we have that a trajectory in the phase-space is such that either it is symmetric with respect to the plane $y = z$ or a symmetric trajectory exists. That is, let $\tau(x_0, y_0, z_0) = \{T^n(x_0, y_0, z_0),\ n \geqslant 0\}$ be the trajectory associated with the initial condition (x_0, y_0, z_0), then either set $\tau(x_0, y_0, z_0)$ is symmetric with respect to the plane $y = z$ (in which case $\tau(x_0, y_0, z_0) = \tau(x_0, z_0, y_0)$), or the trajectory $\tau(x_0, z_0, y_0)$ is symmetric to $\tau(x_0, y_0, z_0)$ with respect to the same plane $y = z$.

In particular, the plane of equation $y = z$ is invariant, or better, mapped into itself. Note that in terms of the three parameters (a, b, c) of the map T this case corresponds to identical characteristic parameters for the last two oligopolists, that is, $b = c$. And it is soon clear that this is not the only case in which we have an invariant plane for the map. In fact, we have a similar property also when $a = b$, that is, in terms of the reduced parameters, when we consider $(1, k)$. It follows that when the parameters are of type (a, a, c) then the plane of equation $x = y$ is invariant and the trajectories of the map T in the phase-space are either symmetric with respect to that plane, or symmetric trajectories exist. Similarly, if we consider the case in which $a = c$, that is, in terms of the reduced parameters $(h, 1)$, then the plane of equation $x = z$ is invariant and the trajectories of the map T in the phase-space are either symmetric with respect to that plane, or symmetric trajectories exist.

Note that this last result can also be obtained from the previous ones. In fact, we have seen that the map with parameters $(1, 1, k)$ (for which $x = y$ is an invariant plane) is topologically conjugated (via the homeomorphism $\psi(x, y, z) = (x, z, y)$) to the map having parameters $(1, k, 1)$, and thus a simple change of the parameter's name gives the desired property (and it follows from the conjugacy that $x = z$ is an invariant plane).

In particular, the restriction of T to an invariant plane can be identified with a 2D map. As we shall see in the following, the restrictions of T to the three invariant planes, in the three cases discussed above, are all topologically conjugated. And also the dynamics of the 3D map T in such cases turn to be conjugated.

The properties evidenced above can also be formulated, perhaps with a clearer applied interpretation, for the map T in terms of terns of the original parameters as follows:

Proposition 4.

(1) *The dynamics of the map T with terns of parameters* (a, b, c) *and* (a, c, b) *are topologically conjugate, via the homeomorphism* $\psi_1(x, y, z) = (x, z, y)$, *and in the case* $c = b$ *the plane* $y = z$ *is invariant with trajectories which are symmetric with respect to that plane or symmetric trajectories exist.*

(2) *The dynamics of the map T with terns of parameters* (a, b, c) *and* (c, b, a) *are topologically conjugate, via the homeomorphism* $\psi_2(x, y, z) = (z, y, x)$, *and in the case* $a = c$ *the plane* $x = z$ *is invariant with trajectories which are symmetric with respect to that plane or symmetric trajectories exist.*

(3) *The dynamics of the map T with terns of parameters* (a, b, c) *and* (b, a, c) *are topologically conjugate, via the homeomorphism* $\psi_3(x, y, z) = (y, x, z)$, *and in the case* $a = b$ *the plane* $x = y$ *is invariant with trajectories which are symmetric with respect to that plane or symmetric trajectories exist.*

Finally we recall the similar properties coming from the rotations of the parameters' values, which imply topological conjugacy in the phase-spaces by using rotations around the axis of equation $x = y = z$:

Proposition 5.

(4) *The dynamics of the map T with terns of parameters* (a, b, c) *and* (c, a, b) *are topologically conjugate, via the homeomorphism* $\psi(x, y, z) = (z, x, y)$.

(5) *The dynamics of the map T with terns of parameters* (a, b, c) *and* (b, c, a) *are topologically conjugate, via the homeomorphism* $\psi^2(x, y, z) = (y, z, x)$.

These properties can also be deduced by composition of two of the conjugacies given in Proposition 4, that is, $\psi_1 \circ \psi_2(a, b, c) = \psi_2 \circ \psi_3(a, b, c) = \psi_3 \circ \psi_1(a, b, c) = (c, a, b)$, and the homeomorphism $\psi = \psi_1 \circ \psi_2 = \psi_2 \circ \psi_3 = \psi_3 \circ \psi_1$ is a rotation of $2\pi/3$ on the right of the oriented vector (1, 1, 1).

While $\psi_2 \circ \psi_1(a, b, c) = \psi_3 \circ \psi(a, b, c) = (b, c, a)$, and the hemeomorphism $\psi^2 = \psi_2 \circ \psi_1 = \psi_3 \circ \psi_2 = \psi_1 \circ \psi_3$ is a rotation $4\pi/3$ on the right (or equivalently of $-2\pi/3$ on the left) of the oriented vector $(1, 1, 1)$.

6. The dynamics of T in the case $a = b$

In this section we consider the particular case in which two of the parameters are equal. As we shall see, any choice of couples of parameters is equivalent from a dynamical point of view, so that let us assume $a = b$. This means that if the initial states of the productions x and y, say x_0 and y_0, are equal, then the two

players will 'move' in the same way forever: $x_t = y_t$ for any $t \geqslant 0$. That is, their response to the market (modified also by the third oligopolist) is always the same. Certainly if their initial states are not equal, then their stories will be different, at least in a transient part, which may also be very short, and it is possible (or highly probable, depending on the structure of the basins) that ultimately they will behave in the same way, or better, that their asymptotic behavior is similar.

Mathematically this comes from the fact that assuming $a = b$, from the first two equations of the map T it is immediately evident that the plane Π^* of equation $y = x$ is trapping, i.e. mapped into itself. Consider a point $p = (u, u, z) \in \Pi^*$, then $T(p) \in \Pi^*$. The plane is called Π^* because it is really the vertical plane through the fixed point E^* and the z-axis, of equation $y = x$ (being $m^* = y^*/x^* = 1$ in this case). Thus all the points belonging to Π^* have the trajectories trapped on that plane, which we shall call *invariant* for short (although it is strictly mapped into itself). It follows that the dynamics of points belonging to Π^* can be studied by use of a simpler map: the restriction of T to that invariant plane, which can be identified with a 2D map. Let us denote by u the common value $x = y$ (as we have already written above in p), then the dynamics of T on Π^* can be reduced to that of the 2D map, say T_u, given by:

$$T_u : \begin{cases} u' = \sqrt{\dfrac{u+z}{a}} - u - z, \\ z' = \sqrt{\dfrac{2u}{c}} - 2u, \end{cases} \tag{15}$$

where a point $(u, z) \in \Pi^*$ identifies the point $(u, u, z) \in \mathscr{R}^3$. The domain D_u of definition of this 2D map is the intersection of the domain of definition of the 3D map T with the plane Π^* (here and in the following, with the index u we denote the restriction of the sets to the invariant plane Π^*), and can also be immediately deduced from its definition in (15):

$$u \geqslant 0,$$
$$u + z \geqslant 0.$$

This region is shown in Fig. 4, where also the critical curves of T_u are represented, as described below.

Let us first consider the fixed point E^*. It belongs to Π^* and its components in the invariant plane become:

$$E^* = (u^*, z^*) = \left(\frac{2c}{(2a+c)^2}, \frac{2(2a-c)}{(2a+c)^2} \right).$$

Clearly, the 2D map T_u also has another fixed point (unstable) in the origin of the plane. Regarding the fixed point of interest, E^*, we can recall the analysis performed in Section 2, obtaining the E^* belongs to the positive quadrant of the plane Π^* provided that the parameters a and c satisfy the conditions given in (7), which now simplify, noticing that one of the reduced parameters is fixed, being $h = 1$. It follows that we are

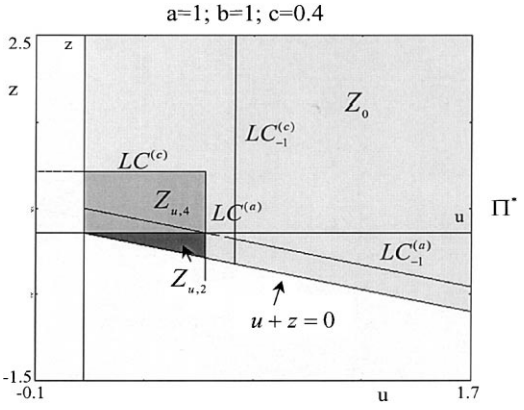

Fig. 4. The domain of definition D_u of the map T_u and its critical curves. The different gray colours represent the regions Z_0 (the lightest), Z_2 (the darkest) and Z_4. Π^* is the invariant plane $y = x$ for the map T, in which we consider the map T_u.

interested in the dynamics of the 2D map T_u as a function of the reduced parameter $k = c/a$, that is, by considering the couple of reduced parameters' value $(1, k)$, and the positivity of the fixed point is ensured by the only condition

$$0 < k < 2.$$

It is also clear that for the stability analysis of the fixed point for the 2D map, we shall get the same results already seen in Section 2 for the 3D map. Thus we can immediately say, by looking at the segment $(1, k)$ for $k < 2$ in the stability region shown in Fig. 1, that the fixed point is attracting for $k_{\text{bif}} < k < 2$, where k_{bif} is the value at which a couple of complex eigenvalues cross the unitary circle. However, the plane Π^* being invariant we have that the couple of eigenvalues associated with the 2D map T_u are necessarily the complex ones. It follows that in this particular case two of the eigenvalues of the Jacobian matrix evaluated at the fixed point can be explicitly determined, as well as bifurcation value k_{bif}. Moreover, as we shall see, this case enables us to recover also the third eigenvalue of T. This is important because our primary interest is that to understand the 3D dynamics of T, also in this particular case in which there is an invariant plane, that is, we are also interested in the fate of trajectories whose initial points are not on Π^*.

Let us consider the Jacobian matrix of T_u, which is suitable also for the critical curves of the 2D map. We have

$$J_{T_u}(u,z) = \begin{bmatrix} \dfrac{1}{2\sqrt{a(u+z)}} - 1 & \dfrac{1}{2\sqrt{a(u+z)}} - 1 \\ \dfrac{1}{\sqrt{2cu}} - 2 & 0 \end{bmatrix} \tag{16}$$

and its evaluation in the fixed point $E^* = (u^*, z^*)$ gives

$$J_{T_u}(u^*,z^*) = \begin{bmatrix} \dfrac{k}{4} - \dfrac{1}{2} & \dfrac{k}{4} - \dfrac{1}{2} \\ \dfrac{1}{k} - \dfrac{3}{2} & 0 \end{bmatrix}$$

so that the characteristic polynomial becomes

$$p_2(\lambda) = \lambda^2 - \left(\frac{k}{4} - \frac{1}{2}\right)\lambda + \frac{3k^2 - 8k + 4}{8k}.$$

The sufficient conditions for the local stability of the fixed point (for this 2D map) are:

(1) $p_2(1) = \frac{1}{2} + \frac{k}{8} + \frac{1}{2k} > 0$ which is always satisfied for $k > 0$,

(2) $p_2(-1) = -\frac{1}{2} + \frac{5k}{8} + \frac{1}{2k} > 0$ which is always satisfied for $k > 0$,

(3) $\det J_{T_u}(u^*, z^*) = ((3k^2 - 8k + 4)/8k) < 1$ which is satisfied only for an interval of values of k, say $k_{\text{bif},1} < k < k_{\text{bif},2}$. By computing $\det J_{T_u}(u^*, z^*) = 1$ we obtain the two bifurcation values $k_{\text{bif},1} = 8 - \sqrt{52}/3 = 0.262966\ldots$ and $k_{\text{bif},2} = 8 + \sqrt{52}/3 = 5.070367\ldots$ In this interval of stability of the fixed point we have in the middle an interval of values at which there correspond a stable node (i.e. the solutions of $p_2(\lambda) = 0$ are real), while near the extrema of the internal of stability, the solutions of $p_2(\lambda) = 0$ are complex conjugate (so that the fixed point is a stable focus) and approach the modulus 1, that is, both the bifurcation values are Neimark–Hopf bifurcations of E^*.

As in this case we are interested in values of k lower than 2 (in order to have E^* in the positive orthant of the space), we have that only one bifurcation is of interest. The fixed point is locally attracting for $k_{\text{bif},1} < k < 2$ and we shall see that at $k_{\text{bif},1} = 0.262966\ldots$ a bifurcation of *subcritical type* shall occur. But let us first complete the local stability analysis of the fixed point for T in the 3D phase-space by computing the third eigenvalue of the 3D Jacobian matrix (clearly we already know that the fixed point is stable also for T). The cubic polynomial defined in (12) can be factorized as follows:

$$p_3(\lambda) = p_2(\lambda)(\lambda - \lambda_3), \quad \lambda_3 = \frac{1}{2} - \frac{k}{4}$$

so that we can say that as k decreases from the value 2, the third eigenvalue of T is always associated with a direction attracting towards the invariant plane, at least locally (near the fixed point), and being $\lambda_3 > 0$ the

trajectories are locally on one side of that plane, i.e. they are not oscillating from one side to the other as it happens with a negative eigenvalue, which implies that the trajectories of points outside the invariant plane and near the fixed point cannot be symmetric with respect to the invariant plane.

The basin of the attracting fixed point E^* on the invariant plane $y = x$ is shown in Fig. 5(a). The white points in that figure represent the set of admissible trajectories in that plane, and all the admissible trajectories are convergent to the fixed point, the gray points in D represent the non-admissible trajectories (i.e. the map is not defined after $m > 0$ iterations, while in the equation region of non-definition, which are the gray points not belonging to D on the left of the line of $u = 0$ and below the line $u + z = 0$, this occurs at $m = 0$). We recall that the reduced parameters of interest are $(1, k)$ with $k < 2$, and for any other value of k between 2 and 0.4 (used in the case of Fig. 5(a)), the basins and the dynamics are qualitatively the same. The boundary of the basin shown in Fig. 5(a) is completely known, we shall see that it is given by the preimages of the z-axis, $u = 0$. Moreover we can see that the critical curves of the map, drawn in Fig. 5(a), are very close to the boundary of the basin. This means that as the parameter k is further decreased, a global bifurcation will occur, which shall cause a drastic change in the structure of the basin. To see this we need the equations of the critical curves and the inverses of the 2D map. Clearly these can be recovered also from the formulas already given in Section 4 for the 3D map T, and considering that the geometrical surfaces intersect the invariant plane in straight lines and curves. However we prefer to deduce these formulas directly from the 2D map.

From the determinant of the Jacobian matrix in (16) we have that the locus $\det J_{T_u}(u, z) = 0$, which, as we know, gives the critical curves LC_{-1} of the 2D map, includes two straight lines (we recall that the notation LC for the critical curves of a 2D map comes from the French term *Ligne Critique*):

$$\mathrm{LC}_{-1}^{(c)}: \quad D_u \cap \left\{ u = \frac{1}{8c} \right\},$$

$$\mathrm{LC}_{-1}^{(a)}: \quad D_u \cap \left\{ u + z = \frac{1}{4a} \right\}.$$

These lines correspond to the intersection of the critical surfaces CS_{-1} with the invariant plane Π^*. In fact, it is easy to see that

$$\mathrm{LC}_{-1}^{(c)} = \mathrm{CS}_{-1}^{(c)} \cap \Pi^*,$$
$$\mathrm{LC}_{-1}^{(a)} = \mathrm{CS}_{-1}^{(a)} \cap \Pi^* = \mathrm{CS}_{-1}^{(b)} \cap \Pi^*.$$

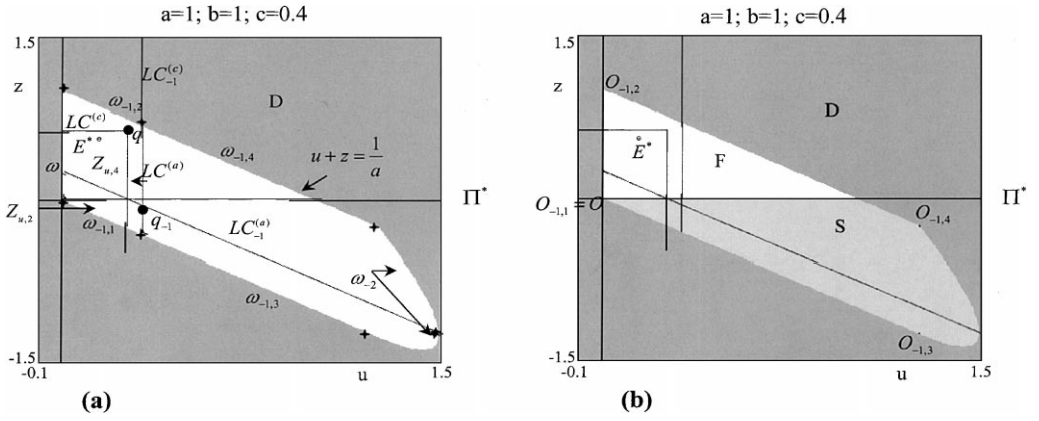

Fig. 5. (a) The basin of the attracting fixed point E^* on the plane Π^*. The white points represent the set of admissible trajectories in that plane (all convergent to the fixed point), the gray points in D represent the non-admissible trajectories. The boundary of the basin is given by the segment ω on the z-axis and its preimages of rank-1, $\omega_{-1,k}$, $k = 1, 2, 3, 4$, and rank-2, ω_{-2}. (b) The light-gray points denote the subset of unfeasible points of the previous basin.

The images of these lines are critical curves of higher rank, in particular we have that the critical curve LC is made up of two half lines, which correspond to the intersection of the critical surfaces CS with the invariant plane Π^*:

$$\mathrm{LC}^{(c)} = \mathrm{CS}^{(c)} \cap \Pi^* : \quad z = \frac{1}{4c} \quad \left(u \leqslant \frac{1}{4a}\right)$$
$$\mathrm{LC}^{(a)} = \mathrm{CS}^{(a)} \cap \Pi^* = \mathrm{CS}^{(b)} \cap \Pi^* : \quad u = \frac{1}{4a} \quad \left(z \leqslant \frac{1}{4c}\right)$$

of which only the portions in D_u are of interest, that is, the segments:

$$\mathrm{LC}^{(c)} : \quad z = \frac{1}{4c} \quad \left(0 \leqslant u \leqslant \frac{1}{4a}\right)$$
$$\mathrm{LC}^{(a)} : \quad u = \frac{1}{4a} \quad \left(-\frac{1}{4a} \leqslant z \leqslant \frac{1}{4c}\right).$$

These curves separate regions with a different number of rank-1 preimages also in the invariant plane. How many of the inverses of T are also inverses of T_u? i.e. taking a point $(u,u,z) \in \Pi^*$ how many of the eight inverses of T belongs to Π^*? To see this we explicitly write the inverses of T_u. Given a point $(u',z') \in \Pi^*$ in the domain of the map, its rank-1 preimages are none if it is 'outside' the critical lines, i.e. $u' > 1/4a$ or $z' > 1/4c$ (see Fig. 4), otherwise four preimages exist when (u',z') belongs to the positive quadrant, and two preimages when $z' < 0$, these preimages are given by:

$$(u^1, z_{1,\pm}) \quad \text{if } (u',z') \in Z_{u,2} = Z_4 \cap \Pi^* \quad \left(0 \leqslant u' < \frac{1}{4a} \text{ and } z' < 0\right)$$
$$(u_1, z_{1,\pm}) \text{ and } (u_2, z_{2,\pm}) \quad \text{if } (u',z') \in Z_{u,4} = Z_8 \cap \Pi^* \quad \left(0 \leqslant u' < \frac{1}{4a} \text{ and } 0 \leqslant z' < \frac{1}{4c}\right),$$

where

$$u_1 = \frac{1}{4c} - \frac{z'}{2} + \frac{\sqrt{1-4cz'}}{4c}, \quad z_{1,\pm} = -u_1 + \frac{1}{2a} - u' \pm \frac{\sqrt{1-4au'}}{2a},$$
$$u_2 = \frac{1}{4c} - \frac{z'}{2} - \frac{\sqrt{1-4cz'}}{4c}, \quad z_{2,\pm} = -u_2 + \frac{1}{2a} - u' \pm \frac{\sqrt{1-4au'}}{2a}.$$

We are now ready to describe the boundary of the basin of attraction of the stable fixed point as long as its basin is a simply connected volume of the 3D space, and thus a simply connected area in the invariant plane. Looking at the basin shown in Fig. 5(a) we consider the boundary of the domain of definition of the map and take its rank-1 primage. This locus completely covers the boundary of the basin. In fact, the vertical axis $u = 0$ belongs to Z_0 except for a small segment in $Z_{u,4}$, for $0 \leqslant z \leqslant 1/4c$ (we include also the critical point $z = 1/4c$ belonging to $\mathrm{LC}^{(c)}$). Let us denote by ω this segment (with extrema on 0 and on $\mathrm{LC}^{(c)}$). Then it has four distinct rank-1 preimages which meet on the critical curve $\mathrm{LC}^{(c)}_{-1}$, see the four segments $\omega_{-1,j}$ for $j = 1,2,3,4$ in Fig. 5(a). Two of them ($\omega_{-1,1}$ and $\omega_{-1,3}$ in Fig. 5(a)) belong to the boundary of the domain of definition, on the line of equation $u + z = 0$, while the other two ($\omega_{-1,2}$ and $\omega_{-1,4}$ in Fig. 5(a)) belong to the line of equation $u + z = 1/a$. Note that all the points of this rank-1 preimage of the segment ω belong to Z_0 except for the segment of $\omega_{-1,1}$ belonging to the boundary of the region $Z_{u,2}$, and that the corners of these segments include the four preimages of the origin on this invariant plane. Taking the two distinct rank-1 preimages of the only segment in $Z_{u,2}$ (with extrema on 0 and $\mathrm{LC}(a)$, belonging to $\omega_{-1,1}$) we obtain two segments, $\omega_{-2,1}$ and $\omega_{-2,2}$, constituting the rank-2 preimages of ω (i.e. $T_u^{-2}(\omega) = \omega_{-2,1} \cup \omega_{-2,2}$), and merging on a critical point of $\mathrm{LC}^{(a)}_{-1}$ (see Fig. 5(a)). Being these last arcs completely included in Z_0, we have ended the boundary (no other preimages of ω exist). Reassuming, taking into account that the segments of interest are the intersections of the boundary of the domain of definition with the Zones, let us call it μ, $\mu = \partial D_u \setminus Z_0$, $\mu \subset \omega \cup \omega_{-1,1}$, we can deduce that it also belongs to the boundary of the region of admissible trajectories S_u, and we have obtained that $\mathscr{B}(E^*)_u = S_u$ and the boundary of the basin is given by $\partial\mathscr{B}(E^*)_u = \partial S_u = \mu \cup T_u^{-1}(\mu)$.

We ought also to know which of these admissible points gives rise to feasible trajectories. We have numerically computed this: the light-gray points in Fig. 5(b) denote the subset of infeasible points of the previous basin. It turns out that the portion of feasible trajectories, that is F_u, is bounded by the preimages of the coordinate axes. In fact, the rank-1 preimage of the u-axis is made up of points belonging to the line $u = 0$ (z-axis) and $u = 1/2c$ (which is completely in Z_0). Thus ∂F_u (the boundary of the white points in Fig. 5(b)) can also be viewed as given by the preimages of rank-1 of the coordinate axes not belonging to Z_0 (which are on the boundary of the feasible trajectories). Defining $\eta = \partial \mathscr{R}^2_+ \setminus Z_0$ we have $\partial F = \eta \cup T_u^{-1}(\eta)$.

We have seen above the local transverse attractivity (near the fixed point) of the invariant plane, with positive transverse eigenvalue in E^*. But we can say also more about the 'attractivity' of the invariant plane, because we can explicitly write the transverse eigenvalue for any point $(u, u, z) \in \Pi^*$, in fact from the Jacobian matrix of T defined in (8) we have (for $a = b$ and $x = y = u$)

$$\lambda_3(u, u, z) = 1 - \frac{1}{2\sqrt{a(u+z)}}.$$

It is immediate to see that above the critical curve $\mathrm{LC}^{(a)}_{-1}$ the transverse eigenvalue is positive while it is negative below it

$$\lambda_3(u, u, z) > 0 \quad \Longleftrightarrow \quad (u+z) > \frac{1}{4a}$$

thus trajectories outside the invariant plane, far from the fixed point, may also 'cross' the plane, while they cannot do this in the region completely above $\mathrm{LC}^{(a)}_{-1}$. Moreover, $\lambda_3(u, u, z) < 1$ is always satisfied, while we have

$$-1 < \lambda_3(u, u, z) \quad \Longleftrightarrow \quad \frac{1}{16a} < (u+z)$$

Thus transverse attractivity exists for a wide portion of Π^*, and as we shall see from our numerical experiments, the attractors of T seem to belong to the region in which we have attractivity for the trajectories starting outside the invariant plane.

Now considering the basin $\mathscr{B}(E^*)$ of the fixed point in the 3D space $\mathscr{R}^3$, we have that it is a simply connected volume, symmetric with respect to the plane $x = y$ (as a consequence of the symmetry property in Proposition 4), whose boundary we conjecture is determined by the rank-1 preimages of the portion of planes defining the boundary of the domain of definition of the map, and not belonging to the region Z_0. That is, the rank-1 preimages of the portions on the planes $y + z = 0,\ x + z = 0,\ x + y = 0$

$$\partial \mathscr{B}(E^*) = \partial S = \mu \cup T^{-1}(\mu), \quad \mu = \partial D \setminus Z_0.$$

Moreover, inside this basin, the set of points having feasible trajectories, i.e. with all the points in the positive orthant, is a simply connected volume in $\mathscr{R}^3_+$, symmetric with respect to the plane $x = y$ and bounded by the rank-1 preimages of the coordinate planes

$$\partial F = \eta \cup T^{-1}(\eta), \quad \eta = \partial \mathscr{R}^3_+ \setminus Z_0.$$

Numerically computed examples are shown in Fig. 6(a)–(c), where we represent the sections on the planes of equation $y = 0.5x$ (which also corresponds to the section on $y = 2x$), $y = 0$ (which also corresponds to the plane $x = 0$), and $z = 0$. As before, white points are feasible (i.e. belong to F), light-gray points are admissible but infeasible (i.e. belong to $S \setminus F$), while the gray points of D are non-admissible.

We note that from Fig. 5(b) it turns out that the region $Z_{u,4}$ is trapping: any other feasible point outside it is mapped in $Z_{u,4}$ in one iteration, and there the trajectory will stay forever, converging to the fixed point. Similarly in the 3D space: any feasible point outside the region Z_8 is mapped inside it in a finite number of iterations and then it converges to the fixed point.

The characteristics of the basin $\mathscr{B}(E^*)$ persist as long as the region Z_8 has no contact with the boundary of the basin. From Fig. 5(a) we can deduce that the point of Z_8 having less distance from the boundary $\partial \mathscr{B}(E^*)$ is the vertex, that is the point $q = (1/4a, 1/4a, 1/4c)$ (which belongs to Π^*). The contact will occur

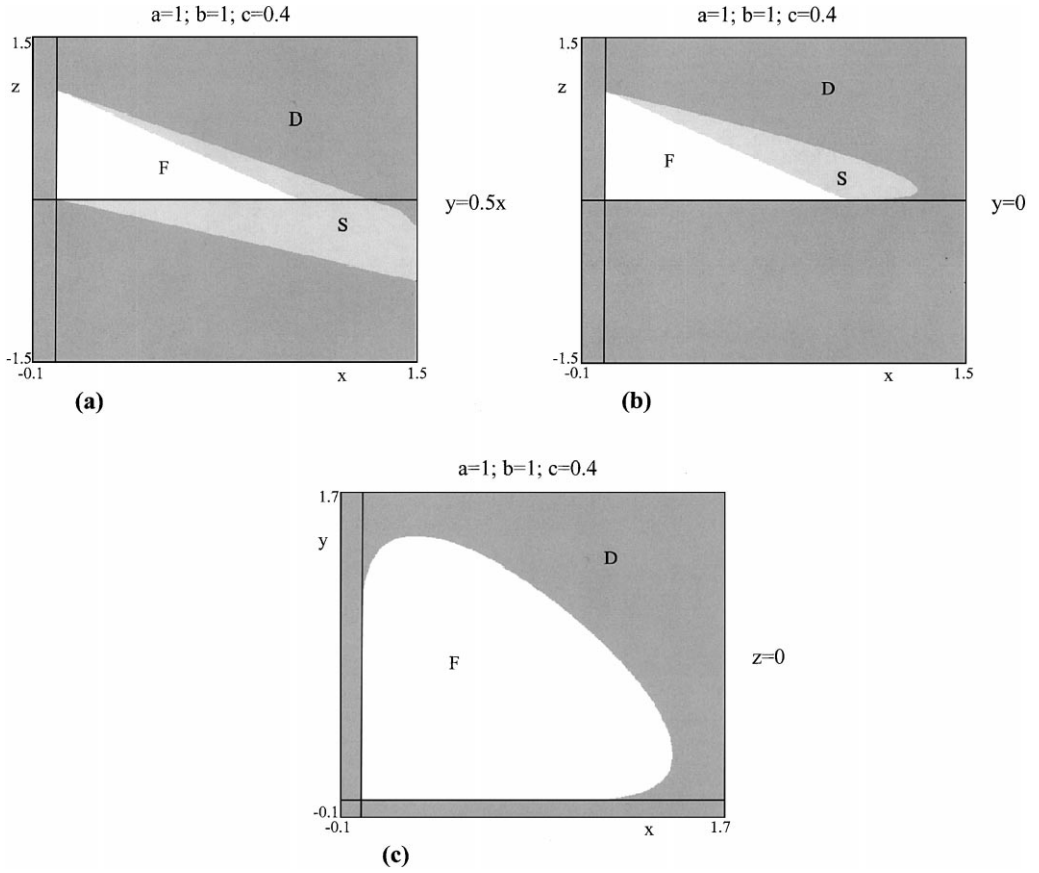

Fig. 6. Three different section of the basin of E^*. The white points denote the feasible region, the light gray points the infeasible one. The gray points in D are non-admissible. (a) Plane section with the plane $y = 0.5x$. (b) Plane section with the plane $y = 0$. (c) Plane section with the plane $z = 0$.

at $k = 1/3$, parameter value at which the critical point q on Π^*, $q = \mathrm{LC}^{(c)} \cap \mathrm{LC}^{(a)}$, also belongs to the line $u + z = 1/a$ defining the boundary of the basin (see Fig. 7(a)). At this bifurcation value the point q has all its four rank-1 preimages on the invariant plane which are merging in the point $q_{-1} = \mathrm{LC}^{(c)}_{-1} \cap \mathrm{LC}^{(a)}_{-1}$.

In the 3D space, the point q is the intersection point of the three critical planes, $q = \mathrm{CS}^{(c)} \cap \mathrm{CS}^{(a)} \cap \mathrm{CS}^{(b)}$, and at the bifurcation value it has all its eight rank-1 preimages merging in the point $q_{-1} = \mathrm{CS}^{(c)}_{-1} \cap \mathrm{CS}^{(a)}_{-1} \cap \mathrm{CS}^{(b)}_{-1}$.

For $k < 1/3$ the region of non-admissible points enter inside Z_4 in the restriction to Π^* (inside Z_8 in the 3D space), see Fig. 7(b), where this portion is labeled by H_u. That is, H_u is bounded by segments of critical curves $\mathrm{LC}^{(c)}$ and $\mathrm{LC}^{(a)}$ near q, and a segment of the basin boundary on the line $u + z = 1/a$. Thus also all the preimages of this area H_u are non-admissible points. For k not far from the bifurcation value the four rank-1 preimages on Π^* are all near the point q_{-1}, constituting, all together, a unique 'hole' $H_{u,-1}$ (i.e., $H_{u,-1} = \cup_{j=1}^{4} H_{u,-1,j}$), which belongs to Z_0, and thus it has no other preimage.

This means, in the 3D space, that for $k < 1/3$ the portion of non-admissible points entering inside Z_8 is a volume, say H (whose intersection with Π^* is the area H_u in Fig. 7(b), i.e. $H_u = H \cap \Pi^*$), bounded by portions of critical planes $\mathrm{CS}^{(c)}, \mathrm{CS}^{(a)}$ and $\mathrm{CS}^{(b)}$ near q, and segments of the basin boundary. Thus also all the preimages of this volume H are non-admissible points. For k not far from the bifurcation value the eight rank-1 preimages of H are all near the points q_{-1}, constituting, all together, a unique 'hole' H_{-1} (i.e., $H_{-1} = \cup_{j=1}^{8} H_{-1,j}$, and its intersection with Π^* is the area $H_{u,-1}$ in Fig. 7(b)) which belongs to Z_0, and thus it has no other preimage.

At $k \simeq 0.32$ another global bifurcation occurs, which shall cause the appearance of other holes of non-admissible points inside the basin $\mathscr{B}(E^*)$ of the fixed point, which continue to be connected but not simply.

At $k \simeq 0.32$ in fact, we can see from Fig. 8(a) that the hole H_{-1} has a contact with the regions $Z_{u,2}$ and $Z_{u,4}$, crossing these regions for lower values of k. Sections of $\mathscr{B}(E^*)$ (we remember that it is symmetric with respect the plane $x = y$) with other planes in the three-dimensional space are shown in Fig. 8(b) and (c), evidencing how the hole H_{-1} is a sort of 'ball' around q_{-1}. In Fig. 8(b) is projected the basin taken on the

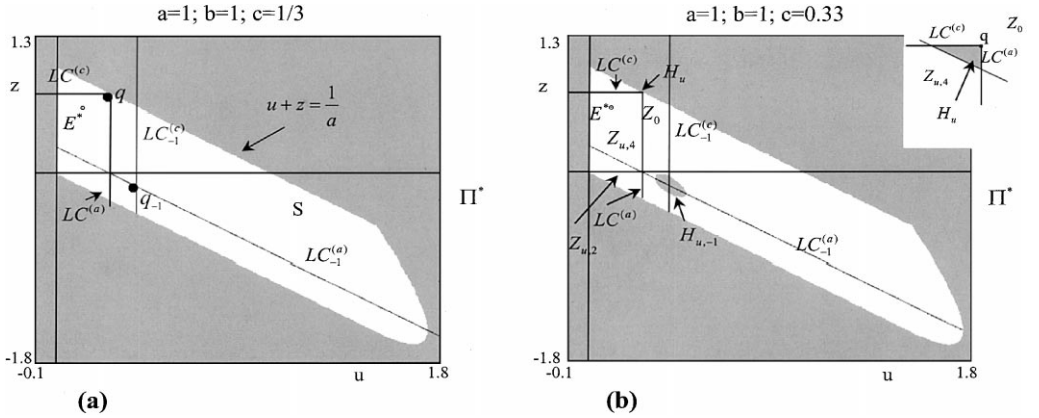

Fig. 7. (a) The critical point q on $\Pi^*, q = \mathrm{LC}^{(c)} \cap \mathrm{LC}^{(a)}$, also belongs to the line $u + z = 1/a$. At this bifurcation value the point q has all its four rank-1 preimages which are merging in the point $q_{-1} = \mathrm{LC}^{(c)}_{-1} \cap \mathrm{LC}^{(a)}_{-1}$. (b) A region H_u of non-admissible points enter inside Z_4. The preimages of this area H_u are non-admissible points and constitute a unique hole $H_{u,-1}$ near the point q_{-1}.

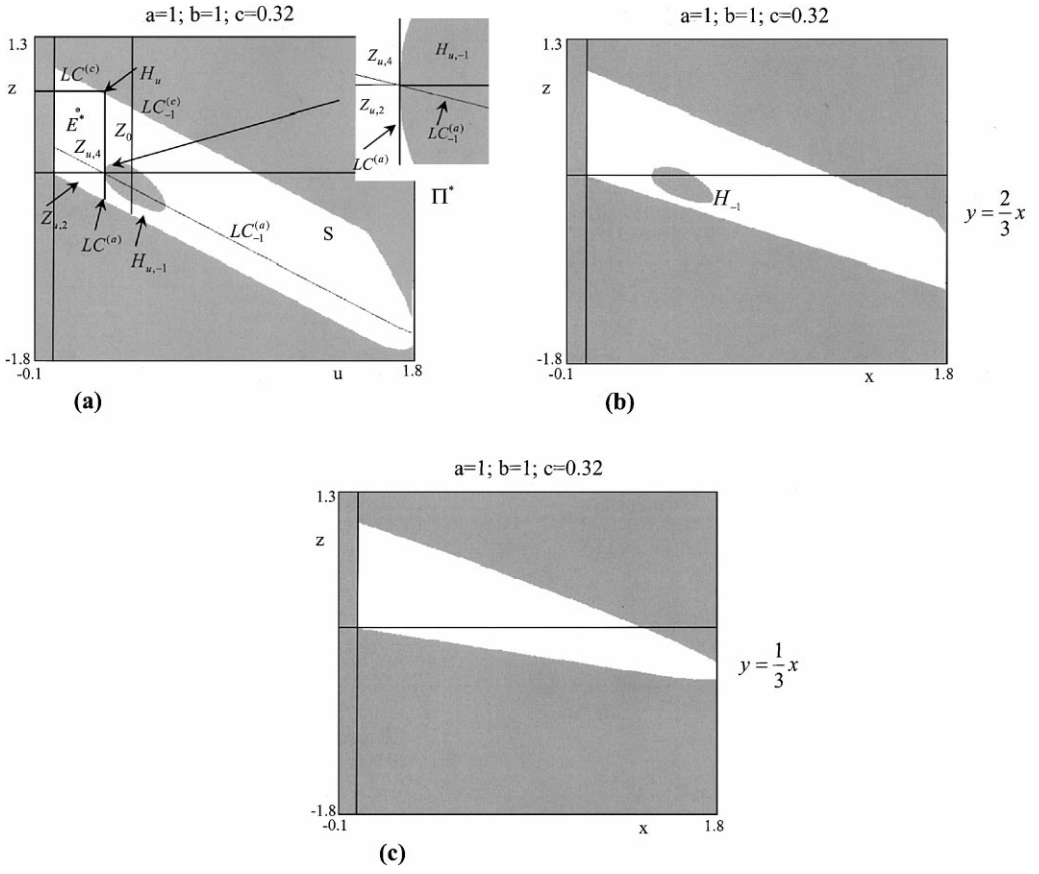

Fig. 8. (a) The hole $H_{u,-1}$ on Π^* has a contact with the regions $Z_{u,2}$ and $Z_{u,4}$, crossing these regions for lower values of k. (b) Plane section of the basin E^* with the plane $y = 2x/3$. (c) Plane section of the basin of E^* with plane $y = x/3$.

plane of equation $y = 2x/3$ (which also corresponds to the section on $y = 3x/2$), and on $y = x/3$ (which also corresponds to the section on $y = 3x$).

While Fig. 9(a) refers to a lower value of k, after the new contact bifurcation, and some of the holes now existing (preimages of $H_{-1} \cap Z_{u,k}$) are emphasized. Really in that figure the preimages of H are to be taken only up to the fourth order, because $T^{-4}(H)$ is completely inside the region Z_0. We have one hole with T^{-1}, two more holes with T^{-2} (one of which is in $Z_{u,4}$ and one in Z_0), four more holes with T^{-3} (one of which is in $Z_{u,2}$ and three in Z_0), finally two more holes with T^{-4} (both in Z_0). Only a few of them are visible in Fig. 9(a) (as before, white points are feasible (i.e. belong to F), light-gray points are admissible but infeasible (i.e. belong to $S \setminus F$), while the gray points of D are non-admissible).

In the 3D space the preimages of the volume H are volumes (inside the old basin $\mathscr{B}(E^*)$) whose dimensions decrease at each preimage. In Figs. 9(b) and (c) we show the projections of the basins on the planes of equation $y = 2x/3$ and $y = x/3$.

These contact bifurcations may increase as the parameter k decreases. Whenever one of the existing holes has a contact with a critical curve LC (boundary of a region Z_k), then the number of preimages (and thus of holes) increases. We note that in any case all the existing holes are obtained by taking the preimages of any rank (as long as these exist) of H, or equivalently of H_{-1} (and for this reason it is also called the 'main' hole, see [1,21]). For example, the hole belonging to $T^{-3}(H)$ located above the region $Z_{u,4}$ which is the upper-leftmost hole, at the beginning is outside the critical line $\mathrm{LC}^{(c)}$, so that it is in Z_0, but then (as k decreases) it becomes wider and a contact with $\mathrm{LC}^{(c)}$ occurs, followed by a crossing, thus creating another main hole, say

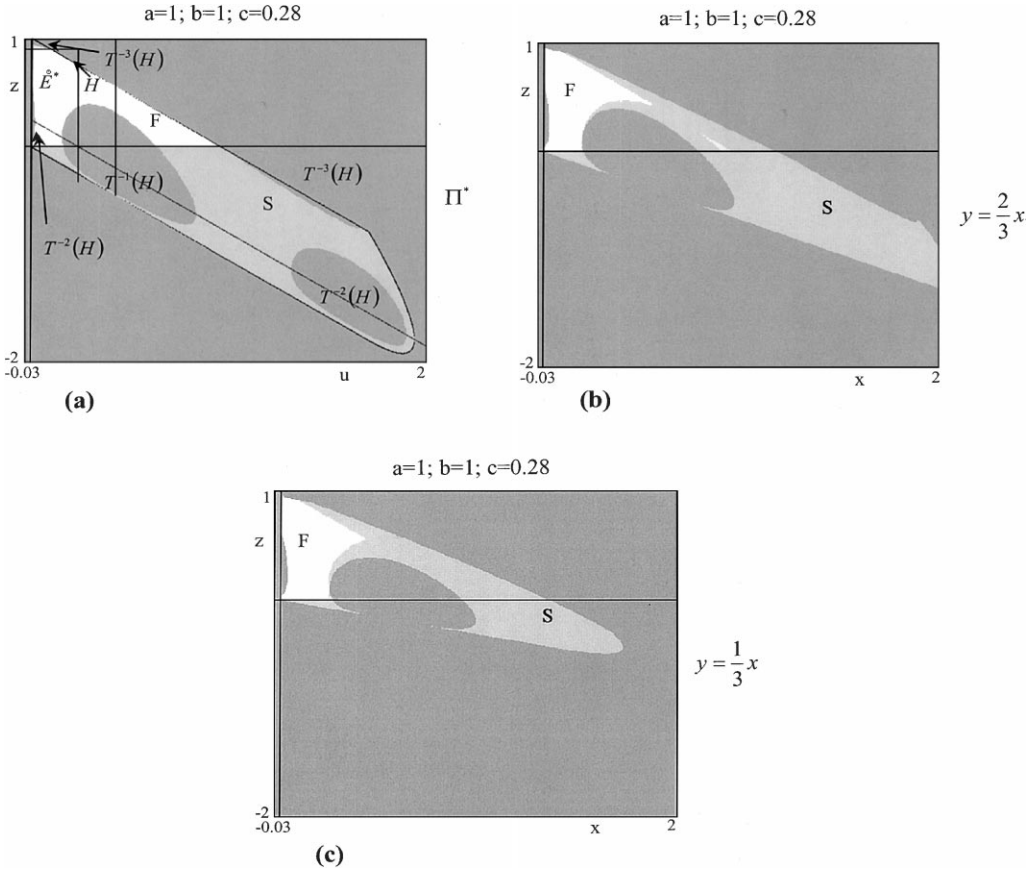

Fig. 9. (a) As the parameter c decreases we have new holes inside the old basin, given by the preimages of any rank of H : only a few of them are visible in figure. As before, white points are feasible, light-gray points are admissible but unfeasible, while the gray points of D are non-admissible. (b) Plane section of the basin of E^* with the plane $y = 2x/3$. (c) Plane section of the basin of E^* with the plane $y = x/3$.

K_{-1} around the critical line $\mathrm{LC}_{-1}^{(c)}$, at first in Z_0. The increase of H_{-1} and of K_{-1} (as the parameter k decreases) gives rise to a basin of the shape shown in Fig. 10(a).

It is clear that now, when 'holes' appear, the boundaries of S and F are determined by taking all the existing preimages of the sets μ and η:

$$\partial S \subseteq \cup_{j\geqslant 0} T^{-j}(\mu), \quad \mu = \partial D \setminus Z_0,$$

$$\partial F \subseteq \cup_{j\geqslant 0} T^{-j}(\eta), \quad \eta = \partial \mathscr{R}^3_+ \setminus Z_0.$$

It is worth noticing that another global bifurcation may occur, causing the transition of the basin $\mathscr{B}(E^*)$ from connected (but not simply, i.e. with holes) to disconnected. This may be due to the reunion of H_{-1} and of K_{-1} and their contact with the lines of equation $u+z=0$ and $u+z=1/a$. However the critical curve $\mathrm{LC}^{(c)}$ intersects the z-axis in the point $(0, 1/4c)$ which is above the line $u+z=1/a$ only for $k<1/4$, and we shall see that the dynamics of interest shall end before (i.e. at a higher value of k). Thus, although the figures seem to show a disconnected basin (due to the roughness of the pixel), it is really a connected one.

One may think that the basin $\mathscr{B}(E^*)$ persists in this shape as k decreases towards its bifurcation value. Indeed this is what occurs when the Neimark–Hopf bifurcation is supercritical, but it is not the case here. It is difficult to say the exact bifurcation value, say $k_f, k_{\mathrm{bif},1} < k_f < 0.264$, at which a global bifurcation occurs

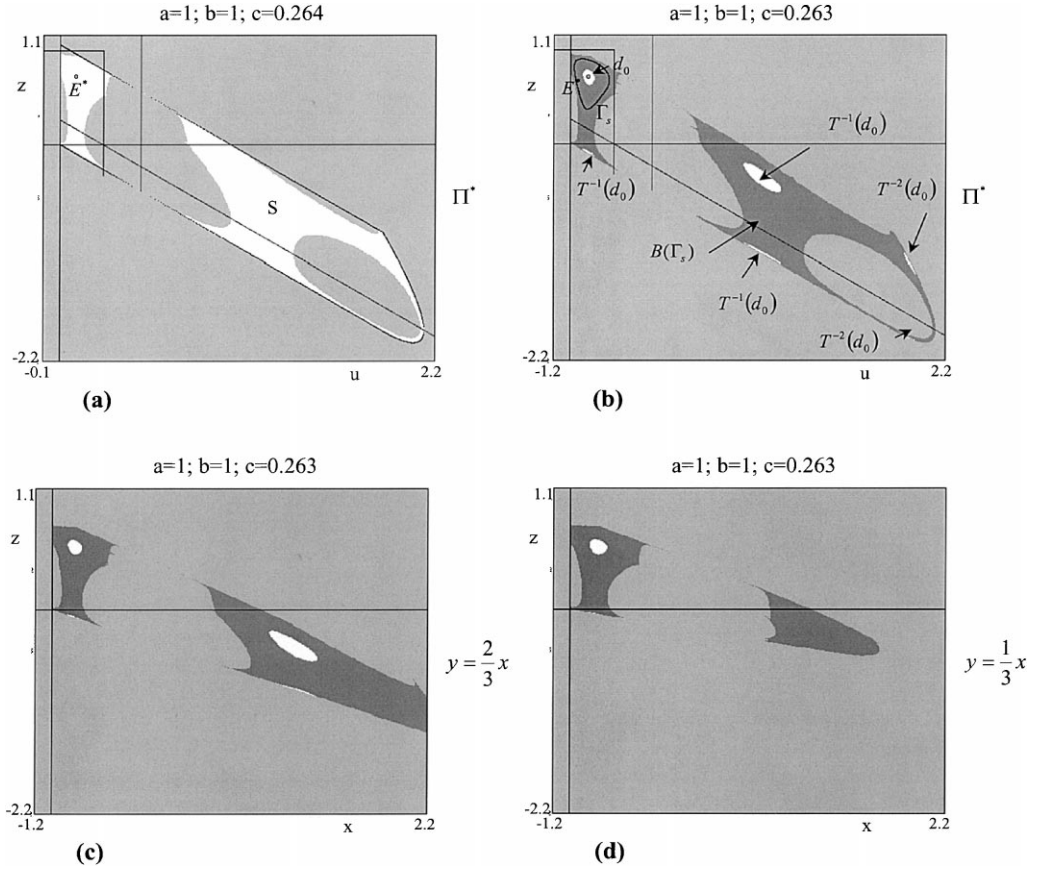

Fig. 10. (a) The holes become wider as c decreases. Although the figures seem to show a disconnected basin (due to the roughness of the pixel), it is really a connected one (but not simply). (b) A global bifurcation occurred giving rise to the birth of two closed invariant curves, one attracting, Γ_s, and one repelling, Γ_u. The fixed point is still attractive. The white points belong to the basin $\mathscr{B}(E^*)$ on the invariant plane, while the dark-gray points belong to the basin $\mathscr{B}(\Gamma_s)$ of Γ_s. The closed repelling curve Γ_u constitute the boundary of the immediate basin d_0 of the fixed point. The total basin of E^* is made up of this immediate basin and its preimages of any rank. (c) Plane section of the basins with the plane $y=2x/3$. (d) Plane section of the basins with the plane $y=x/3$.

giving rise to the birth of two closed invariant curves, one attracting, Γ_s, and one repelling, Γ_u. That this is the case is a numerical evidence, which shows two coexisting attractors, namely the fixed point and a closed invariant curve (see Fig. 10(b)). The white points in that figure belong to the basin $\mathscr{B}(E^*)$ on the invariant plane, while the dark-gray points belong to the basin $\mathscr{B}(\Gamma_s)$ of a closed invariant curve Γ_s also visible in the same figure. Due to the invariance of the plane Π^* the two invariant curves Γ_s and Γ_u must belong to it. It is clear that now the closed repelling curve Γ_u constitute the boundary of the immediate basin of the fixed point, say d_0 this area bounded by Γ_u. The total basin being made up of this immediate basin and its preimages of any rank, which in our example are only two: $T^{-1}(d_0)$ consists of four sets, one of which is in $Z_{u,2}$ and the others in Z_0, then $T^{-2}(d_0)$ consists of two more sets, both in Z_0, thus no other points can be obtained (i.e. $T^{-3}(d_0) = T^{-2}(d_0)$) (see Fig. 10(b)).

Regarding the behavior of the points in the 3D space we can see from the sections on other planes (Fig. 10(c) and (d)) that the basin $\mathscr{B}(E^*)$ is made up of only six disconnected volumes, bounded by the stable set of Γ_u, $W^s(\Gamma_u)$. All the other points, previously (i.e. for $k > k_f$) in the basin of the fixed point now converge to a different attractor. The gray points always denote the non-admissible trajectories.

In order to see which are the feasible points in this new situation we denote by different colors such points (see Fig. 11). The basin $\mathscr{B}(E^*) \cap \mathscr{R}^3_+$ is made up of feasible trajectories, and is colored in white in Fig. 11, while its infeasible trajectories are in red. The feasible trajectories converging to Γ_s are colored in green while those infeasible in light blue.

The set $\mathscr{B}(E^*) \cap \mathscr{R}^3_+$ is very small and, on decreasing k, it will disappear completely because the invariant curve Γ_u decreases in size and shrinks to the fixed point at the Neimark–Hopf bifurcation value of subcritical type $k = k_{\mathrm{bif},1} = 0.262966$. After the bifurcation, for $k < k_{\mathrm{bif},1}$, the fixed point becomes unstable and the only surviving attractor is Γ_s on the invariant plane. Fig. 11 shows that the distance of Γ_s from the repelling focus E^* increases as k decreases, and we can also observe the occurrence of a non-linear phenomena on the shape of the curve Γ_s caused by the non-invertibility of the map. In fact, it is well known that the crossing of Γ_s through the critical curve LC_{-1} causes the appearance of 'oscillations' in the geometrical shape of the curve (see e.g. [21,23]), due to the 'foldings' of the curve which must occur on LC. This occurs, in our example, when Γ_s crosses $\mathrm{LC}^{(a)}_{-1}$, which implies the tangency of Γ_s in two points of $\mathrm{LC}^{(a)}$, and smooth oscillations appear on its shape (see Fig. 12). Clearly these tangential points of Γ_s with $\mathrm{LC}^{(a)}$ also persist in the forward images, so that Γ_s is tangent also to the critical curves $\mathrm{LC}^{(a)}_j$, $j \geqslant 0$.

Moreover, following the procedure described in [21], we can find an absorbing area in the invariant plane Π^*, bounded by a finite number of critical arcs. Let us show this at a lower value of k. As it is expected, when the parameter c decreases the attractors on the closed invariant curve Γ_s modify. At first we have, on Γ_s, either an attracting cycle (and the set Γ_s is a heteroclinic connection, or saddle-node connection), or quasi-periodic motions occur (all the trajectories are dense on the curve Γ_s) (see also [23]). But far from the bifurcation value other non-linear phenomena appear, which cause the destruction (or disappearance) of

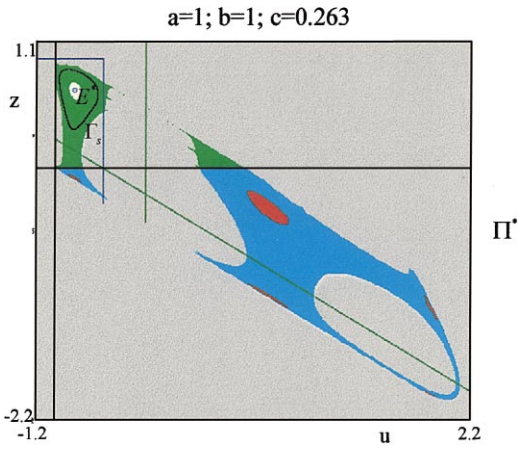

Fig. 11. The same case as Fig. 10(b), but here the feasible points in $\mathscr{B}(E^*)$ are coloured in white, while its unfeasible trajectories are in red. The feasible trajectories converging to Γ_s are colored in green while those unfeasible in blue.

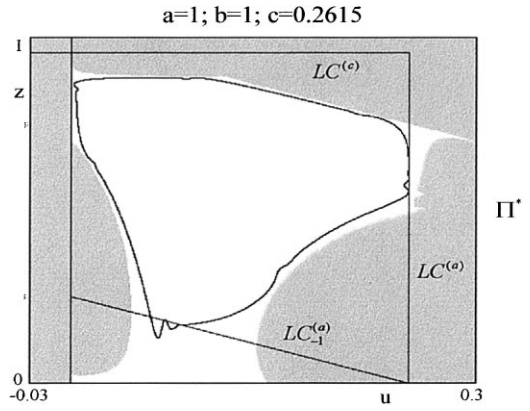

Fig. 12. After the subcritical Neimark–Hopf bifurcation, the fixed point becomes unstable and the only surviving attractor is Γ_s on the invariant plane. In our example, Γ_s crosses $LC^{(c)}_{-a}$, this implies the tangency of Γ_s in two points of $LC^{(a)}$, and smooth oscillations appear on its shape.

the closed invariant curve, leading to a different attracting set. In our example, as often occurs, we have the appearance of a cycle which undergoes a flip bifurcation, on its turn followed by a sequence of flip bifurcations, leading to chaotic dynamics. The attracting set shown in Fig. 13(b) is already in this chaotic regime, and it belongs to an absorbing area V_u. A small segment of $LC^{(a)}_{-1}$, crossed by the attractor, and given exactly by $\gamma = V_u \cap LC^{(a)}_{-1}$, is taken as 'germ' to obtain the boundary, being $\partial V_u \subset \cup_{j=1}^{7} T^j(\gamma)$, and ∂V_u is made up of seven critical arcs belonging to $LC^{(a)}_{-1+j}$, $j = 1, \ldots, 7$. In Fig. 13(a) only the absorbing area is shown, while in Fig. 13(b) also the attractor inside it is drawn. By increasing the number of images it is also possible to define an annular area, say $V_{a,u}$, containing the attracting set. Inside the annular area there is the repelling focus E^*, and the trajectories of the points in the internal part $V_u \setminus V_{a,u}$, except for E^* shall enter the annular area in a finite number of iterations, and then they cannot escape from it (being $T(V_{a,u}) \subseteq V_{a,u}$).

It is clear that we can repeat the above construction also for the 3D map, obtaining an absorbing volume V and an annular volume V_a. Selecting a portion of plane on $CS^{(a)}_{-1}$ which is crossed by the attractor (and exactly taking $\gamma = V \cup CS^{(a)}_{-1}$), we can obtaining the boundary of an absorbing volume which is made up of portions of critical surfaces belonging to $CS^{(a)}_{-1+j}$, $j = 1, \ldots, 7$ (being $\partial V \subset \cup_{j=1}^{7} T^j(\gamma)$). Moreover, by increasing the number of images, we can obtain an annular volume (often homeomorphic to a torus), always bounded by portions of critical surfaces.

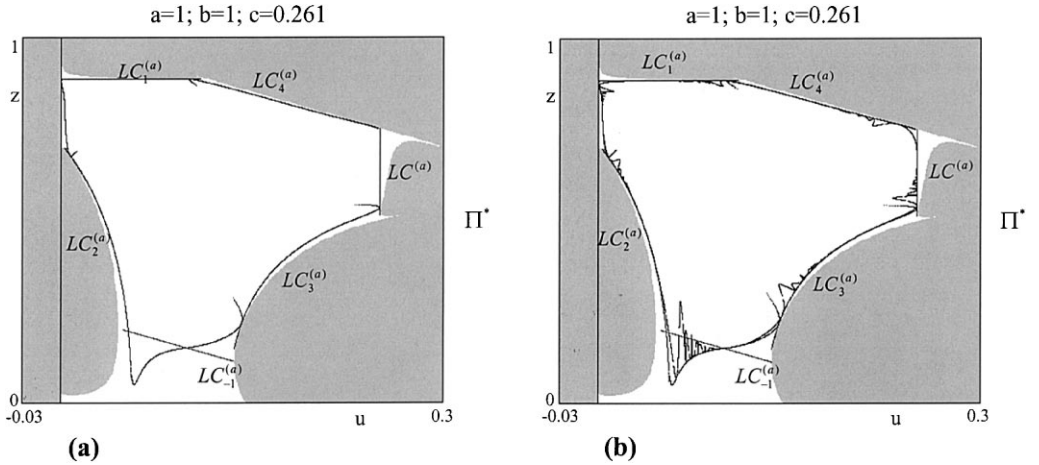

Fig. 13. Chaotic set in the invariance plane Π^* obtained by decreasing the parameter c. (a) The absorbing area whose boundary is made up of seven critical arcs belonging to $LC^{(a)}_{-1+j}$, $j = 1, \ldots, 7$. (b) The attractor inside the absorbing area.

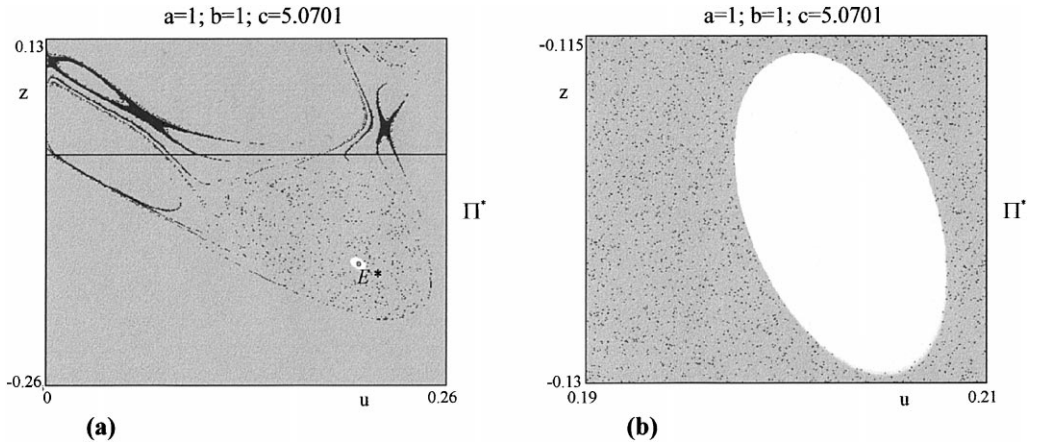

Fig. 14. A different regime: $c > 2$. (a) A stable 6-cycle together with the stable fixed point E^*. The gray points denoted the non-admissible trajectories, the green points the basin of the 6-cycle and the white ones the basin E^*. (b) Enlargement of the immediate basin of E^*: the smooth shape of the basin boundary suggests the existence of a repelling closed invariant curve Γ_u on Π^*.

As k decreases the attracting set cross the coordinate plane $z = 0$ thus becoming admissible but unfeasible. This crossing also marks the approximation of the attracting set to the boundary of its basin of attraction (which is also the boundary of the admissible points). A contact of the attracting set with ∂S shall cause the disappearance of the attractor leaving a strange repellor and almost all (i.e. except for a set of Lebesque zero measure) non-admissible points.

Before closing this section, we shall also make some remarks on the behavior of the dynamics of T for values of k higher than 2. Although this is not interesting in the applied context, it may be interesting, from a dynamical point of view, the analysis of the type of Neimark–Hopf bifurcation occurring on other branches of the bifurcation curve (see for $h = 1$ the other intersection on the curve of Fig. 1, which occurs at $k = k_{\text{bif},2} = 5.070367\ldots$ In this different regime ($k > 2$) other bifurcations of the basin of attraction $\mathscr{B}(E^*)$ occurs, of the same type as those described in this section, due to contacts and crossing of the critical curves which separate the zones Z_k. These bifurcations cause the decreasing in size of the set of admissible trajectories, which is equal to the basin of E^* as long as it is the only attractor. In fact, other bifurcations cause the appearance of stable attracting sets of T, coexisting with E^* stable. We have detected a 6-pieces cyclical chaotic set which (on increasing k) undergoes reverse bifurcations which end in a cycle of period 6. In Fig. 14(a) we can see a stable 6-cycle together with the stable fixed point E^*. Although the gray points in that figure are already many (due to the increasing in size of holes of non-admissible trajectories), also in this regime a global bifurcation causes the reduction of the basin of the fixed point, due to 'competition' with another attractor, occurring before the Neimark–Hopf bifurcation. Now the boundary separating the basin of E^* from the basin of the 6-cycle may also have a fractal structure, however, enlarging the region near the fixed point we see Fig. 14(b) that the basin boundary (of the white points) has a smooth shape, thus suggesting the existence of a repelling closed invariant curve Γ_u on the invariant plane defining this boundary. As k approaches the bifurcation value $k_{\text{bif},2}$, this area shrinks, merging with the fixed point at $k = k_{\text{bif},2}$, Thus also in this case the Neimark–Hopf bifurcation seems to be of subcritical type. After the bifurcation, for $k > k_{\text{bif},2}$, trajectories starting near the repelling focus are unfeasible. In this situation, most parts of the points in the domain D of the map are unfeasible.

7. The dynamics of T in the cases $a = c$ or $b = c$

The dynamics of T when two other parameters are equal, are conjugated to the one described in Section 6. For applied purposes we shall explicitly write here the relations.

Let us first consider the case $a = c$. Now the invariant plane, say Π, is $x = z$, and the restriction of T to that plane reads:

$$T_v : \begin{cases} v' = \sqrt{\frac{v+y}{a}} - v - y, \\ z' = \sqrt{\frac{2v}{b}} - 2v, \end{cases}$$

where a point $(v, y) \in \Pi$ identifies the point $(v, y, v) \in \mathscr{R}^3$. It is evident that changing (u, z) with (v, y) and the parameter c with b, the 2D map T_u in Section 6 becomes the map T_v. In terms of the reduced parameters now we are interested in the values of the couple $(h, 1)$ (being $c/a = 1$ constant), and identifying the parameter h with the parameter k of Section 6, all the bifurcation values are the same as those occurring for k. That is,

$$E^* = (v^*, y^*) = \left(\frac{2b}{(2a+b)^2}, \frac{2(2a-b)}{(2a+b)^2} \right)$$

is positive iff

$$0 < h < 2$$

and attracting for

$$h_{\text{bif},1} < h < h_{\text{bif},2},$$

where $h_{\text{bif},1} = 8 - \sqrt{52}/3 = 0.262966\ldots$ and $h_{\text{bif},2} = 8 + \sqrt{52}/3 = 5.070367\ldots$ The third eigenvalue of T is

$$\lambda_3(v, y, v) = 1 - \frac{1}{2\sqrt{a(v+y)}},$$

$$\lambda_3(E^*) = \frac{1}{2} - \frac{h}{4},$$

and the same considerations of Section 6 hold.

Reassuming, the dynamics of T in the case of parameters (a, b, a) are topologically conjugated to those of the map with parameters $(1, b/a, 1) = (1, h, 1)$ (via the homeomorphism ϕ in Proposition 3, with $\tau = 1/a$), and this last one is, in its turn, topologically conjugated to the map with parameters $(1, 1, h)$ (via the homeomorphism ψ_1 in Proposition 4). Thus the dynamics of the map T with parameters $(a, b, c$ are topologically conjugated (via the hemeomorphism $\psi_1 \circ \phi$) to the dynamics already described in Section 6 (changing the name of the reduced parameter k into h).

Similarly, let us consider now the case of the map T with parameters (a, b, b). It is clear that its dynamics are topologically conjugated (via the homeomorphism ϕ in Proposition 3, with $\tau = 1/b$), to the one with parameters $(a/b, 1, 1) = (1/h, 1, 1)$ which, in its turn, is topologically conjugated to the map with parameters $(1, 1, 1/h)$ (via the homeomorphism ψ_2 in Proposition 4). It follows that by identifying k with $1/h$ (or, equivalently h with $1/k$), the dynamics of the map already described in Section 6 hold also for this case (i.e. T with parameters (a, b, b), via the conjugacy $\psi_2 \circ \phi$). The invariant plane Π is now $y = z$, and the 2D map on that plane reads:

$$T_w : \begin{cases} x' = \sqrt{\frac{2w}{a}} - 2w, \\ w' = \sqrt{\frac{x+w}{b}} - x - w, \end{cases}$$

where a point $(x, w) \in \Pi$ identifies the point $(x, w, w) \in \mathscr{R}^3$. It is evident that reading x, w, a, and b of this map as z, u, c, and a, respectively, we obtain the map already studied in Section 6. So that we can consider the 3D map T, as well as the 2D map T_w on the invariant plane, as a function of the reduced parameters (h, h), where $h = b/a$. Now the fixed point is

$$E^* = (x^*, w^*) = \left(\frac{2(2b-a)}{(a+2b)^2}, \frac{2a}{(a+2b)^2} \right)$$

it is positive iff

$$0 < \frac{1}{h} < 2$$

that is iff

$$\frac{1}{2} < h < +\infty$$

and it is stable for

$$k_{\text{bif},1} = 0.262966 < \frac{1}{h} < k_{\text{bif},2} = 5.070367\ldots$$

that is for

$$\frac{1}{5.070367} = 0.19722\ldots < h < \frac{1}{0.262966} = 3.80277\ldots$$

As we are interested in values of h greater than 0.5 (to have a positive fixed point), the bifurcation occurring at lower values is not interesting (it corresponds to the supercritical bifurcation already described at the end of Section 6), while as h increases above 0.5 we have the same dynamics described for the map T_u in Section 6 (on decreasing k from 2). The third eigenvalue of T is given by

$$\lambda_3(x, w, w) = 1 - \frac{1}{2\sqrt{b(x+w)}},$$

$$\lambda_3(E^*) = \frac{1}{2} - \frac{1}{4h},$$

and the dynamics are attracted to the invariant plane $y = z$.

8. Again the 3D model without invariant plane

Now let us turn to the 3D map T in the generic case in which the three parameters (a, b, c) are all distinct, and we refer to the bifurcation curves in Fig. 1 in terms of the reduced parameters $(h, k) = (b/a, c/a)$. We have investigated the crossing of the bifurcation curves in several points, both in the lower arc as well as in the upper one, and we have always detected a Neimark–Hopf bifurcation of *subcritical type*.

The dynamics of T as the reduced parameters (h, k) exist from the stability region shown in Fig. 1 are qualitatively the same as that we have described in the particular case of Section 6 with $a = b$. Clearly, out of the symmetric case an invariant plane no longer exist, but the dynamics in the phase-space and their bifurcations can be explained in the same way (i.e. by use of the same techniques). For example, the simply connected basin of the fixed point shown in Fig. 15(a) for $(a, b, c) = (1, 0.9, 0.35)$ strictly includes the region Z_8 and the vertex q of that region is below the boundary. We conjecture that the basin of the region S is again determined by taking the preimages of the boundary of D (the domain of definition), as it was in Section 6, that is, the rank-1 preimages of the portions of planes $y + z = 0,\ x + z = 0,\ x + y = 0$, not belonging to Z_0

$$\partial\mathscr{B}(E^*) = \partial S = \mu \cup T^{-1}(\mu), \quad \mu = \partial D \setminus Z_0.$$

Moreover, in Fig. 15(a) the feasible points are drawn in white, and again the boundary of F (which is here simply a connected volume in $\mathscr{R}^3_+$) is given by the preimages of the coordinate planes

$$\partial F = \eta \cup T^{-1}(\eta), \quad \eta = \partial\mathscr{R}^3_+ \setminus Z_0.$$

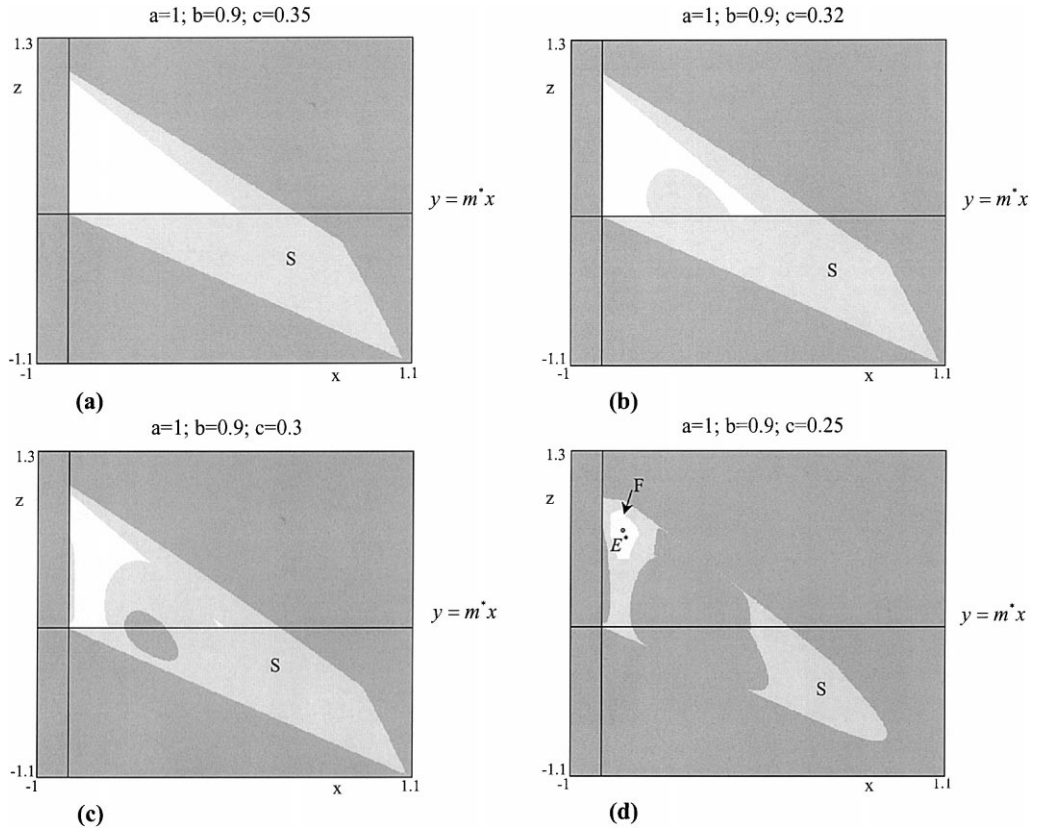

Fig. 15. The generic case, without the invariant plane. (a) The simply connected basin of the fixed point projected on the plane Π^* through the fixed point, and not invariant. The feasible points are drawn in white and the infeasible ones in light-gray. (b) The contact between the critical point q and the boundary of F modified the region of feasible points. (c) A hole of non-admissible points (the gray ones) inside the region $F \subset S$ due to a contact between the point q and the boundary of S. (d) On decreasing the parameter c, the set of admissible trajectories undergoes the same qualitative bifurcation as in the case with invariant plane: the main difference is in the set of feasible trajectories (the light-gray points are the unfeasible ones).

It is clear that the sets described above shall undergo a global bifurcation when the vertex of q of the region Z_8 will have a contact with the boundary of those region, followed by a crossing. Obviously the first contact will be between q and ∂F, modifying the region of feasible points, as shown in Fig. 15(b), where we project the basin computed on the plane Π^* (through the fixed point, and not invariant). A second bifurcation shall occur when (on decreasing c) the point q inside the region $F \subset S$ (see Fig. 15(c)). Thus the set of admissible trajectories undergoes the same qualitative bifurcation as in the symmetric case, with the holes that modify, increasing in number and size, as the parameters are changed. As stated in Section 6, after the appearing of holes, for the boundaries we have:

$$\partial S \subseteq \cup_{j \geqslant 0} T^{-j}(\mu), \quad \mu = \partial D \setminus Z_0,$$

$$\partial F \subseteq \cup_{j \geqslant 0} T^{-j}(\eta), \quad \eta = \partial \mathscr{R}^3_+ \setminus Z_0.$$

The main difference is in the set of feasible trajectories. For example, in the case shown in Fig. 3(b) the set F of feasible trajectories is the white set reported in Fig. 15(d) (the light-gray points are the infeasible ones).

The asymmetry implies the nearness of the attractors to the boundaries of the coordinate-planes, and then a crossing as the parameters are changed. An example was shown in Fig. 3(d) where a chaotic attractor crosses the plane $x = 0$, so that we have all unfeasible trajectories.

Similarly, the holes of the basins shown in Fig. 2 are due to contacts of ∂S with the critical surfaces and boundaries of zones. In Fig. 2(a) we see a small portion of non-admissible trajectories which has crossed the frontier of Z_4 entering Z_8 through the coordinate plane $z = 0$. Such a crossing creates other portions of non-admissible trajectories, but not inside the region Z_8, all the rank-1 preimages of that portion (which are now 8 and all distinct) are located outside the region Z_8. The crossing of that boundary (∂Z_4 in common with ∂Z_8 through a coordinate plane) gives rise to an increase of 4 rank-1 preimages, but not located near critical planes CS_{-1}, while all these are distinct and near the boundary of D in the regions Z_4 (all having at least one negative component). While the usual contact bifurcation creates the hole inside Z_8 shown in Fig. 2(b), that is, this is due to the contact of ∂Z_8 (in the point q) with ∂S, with the same mechanism described in Section 6.

Also the absorbing volumes can be obtained, although it is difficult for us to draw the pictures. Taking a portion of critical plane CS_{-1}, specially when it is crossed by the attracting set, and taking a finite number of images by T, the portions of critical surfaces define a closed absorbing volume V which is mapped into itself by T. An example was shown in Fig. 3(e) where by seven images of a portion of $CS_{-1}^{(a)}$, a volume V can be obtained, and also an annular volume V_a (with more critical surfaces on the boundary).

Acknowledgements

We thank Gian Italo Bischi for helpful comments and Paolo Tenti for the Visual Basic graphical programs. This work has been performed under the auspices of CNR, Italy, under the auspices of Swedish Transport and Communication Research Board, Sweden, and under the activity of the national research project ''Nonlinear Dynamics and Stochastic Models in Economics and Finance'', MURST, Italy.

References

[1] Abraham R, Gardini L, Mira C. Chaos in discrete dynamical systems (a visual introduction in two dimensions). Berlin: Springer; 1997.
[2] Agiza HN. On the analysis of stability, bifurcation, chaos and chaos control of Kopel map. Chaos, Solitons & Fractals 1999;10(11):1909–16.
[3] Agiza HN, Bischi GI, Kopel M. Multistability in a dynamic Cournot game with three oligopolists. Math Comp Simulat (in press).
[4] Ahmed E, Agiza HN. Dynamics of a Cournot game with n competitors. Chaos, Solitons & Fractals 1998;9:1513–7.
[5] Agliari A, Gardini L, DelliGatti D, Gallegati M. Global dynamics in a nonlinear model for the equity ratio. Chaos, Solitons & Fractals 2000;11(6):961–85.
[6] Cournot A. Recherche sur le principes matématiques de la théorie de la richesse. Paris: Hachette; 1838.
[7] Bischi GI, Gardini L. Cycles and bifurcations in duopoly games. Quaderni dell'Istituto di Matematica ''E. Levi'', Università di Parma, no. 3 1998.
[8] Bischi GI, Gardini L, Kopel M. Analysis of global bifurcations in a market share attraction model. J Econom Dynam Contr, submitted for publication.
[9] Bischi GI, Gallegati M, Naimzada A. Symmetry-breaking bifurcations and representative firm in dynamic duopoly games. Ann Oper Res 1999;89:253–72.
[10] Bischi GI, Kopel M. On the basins of multiple Nash equilibria in nonlinear duopoly games, submitted for publication.
[11] Bischi GI, Mammana C, Gardini L. Multistability and cyclic attractors in duopoly games. Chaos, Solitons & Fractals 2000;11(4):543–64.
[12] Bischi GI, Naimzada A. Global analysis of a dynamic duopoly game with bounded rationally. Advances in dynamic games and applications, vol. 5, Boston: Birkhauser.
[13] Bischi GI, Stefanini L, Gardini L. Synchronization, intermittency and critical curves in a duopoly game. Mathematics Computers Simulation 1998;44:559–85.
[14] Devaney R. An introduction to chaotic dynamical systems. Menlo Park: Benjamin; 1986.
[15] Gandolfo G. Economic dynamics, methods and models. Amsterdam: North-Holland; 1980.
[16] Guckenheimer J, Holmes P. Nonlinear oscillations dynamical systems and bifurcations of vector fields. Berlin: Springer, 1983.
[17] Gumowski I, Mira C. Dynamique chaotique. Toulose: Cepadues Editions; 1980.
[18] Collet P, Eckmann JP. Iterated maps on the interval as dynamical systems. Boston: Birkhauser; 1980.
[19] Kopel M. Simple and complex adjustment dynamics in Cournot duopoly models. Chaos, Solitons & Fractals 1996;7:2031–48.
[20] Kopel M, Bischi GI, Gardini L. On new phenomena in dynamic promotional competition models with homogeneous and quasi-homogeneous firms. In: DelliGatti D, Gallegati M, Kirman A, editors. Market structure, aggregation and heterogeneity. Cambridge: Cambridge University Press (in press).
[21] Mira C, Gardini L, Barugola A, Cathala JC. Chaotic dynamics in two-dimensional noninvertible maps. Singapore: World Scientific; 1996.

[22] Mira C, Fournier-Prunaret D, Gardini L, Kawakami H, Cathala JC. Basin bifurcations of two-dimensional noninvertible maps: fractalization of basins. Int J Bifurc Chaos 1994;4:343–81.
[23] Frouzakis CF, Gardini L, Kevrekidis YG, Millerioux G, Mira C. On some properties of invariant sets of two-dimensional noninvertible maps. Int J Bifurc Chaos 1997;7(6):1167–94.
[24] Puu T. Chaos in duopoly pricing. Chaos, Solitons & Fractals 1991;1(6):573–81.
[25] Puu T. Complex dynamics with three oligopolists. Chaos, Solitons & Fractals 1996;7:2075–81.
[26] Puu T. The chaotic duopolists revisted. J Economic Behaviour Organization 1998;33:385–94.
[27] Puu T. Nonlinear economic dynamics. Berlin: Springer; 1997.
[28] Rand D. Exotic phenomena in games and duopoly models. J Math Econom 1978;5:173–84.